Monthly Notices of the ROYAL ASTRONOMICAL SOCIETY

MNRAS **475,** 3098–3116 (2018) doi:10.1093/mnras/stx3249
Advance Access publication 2017 December 20

A view of the *H*-band light-element chemical patterns in globular clusters under the AGB self-enrichment scenario

F. Dell'Agli,[1,2]★ D. A. García-Hernández,[1,2] P. Ventura,[3] Sz. Mészáros,[4,5] T. Masseron,[1,2] J. G. Fernández-Trincado,[6,7] B. Tang,[6] M. Shetrone,[8] O. Zamora[1,2] and S. Lucatello[9]

[1]*Instituto de Astrofísica de Canarias, Vía Láctea s/n, E-38205 La Laguna, Tenerife, Spain*
[2]*Departamento de Astrofísica, Universidad de La Laguna (ULL), E-38206 La Laguna, Spain*
[3]*INAF – Osservatorio Astronomico di Roma, Via Frascati 33, I-00040, Monte Porzio Catone (RM), Italy*
[4]*ELTE Eötvös Loránd University, Gothard Astrophysical Observatory, Szombathely, Hungary*
[5]*Premium Postdoctoral Fellow of the Hungarian Academy of Sciences*
[6]*Departamento de Astronomía, Casilla 160-C, Universidad de Concepción, Concepción, Chile*
[7]*Institut Utinam, CNRS UMR6213, Univ. Bourgogne Franche-Comté, OSU THETA, Observatoire de Besançon, BP 1615, F-25010 Besançon Cedex, France*
[8]*University of Texas at Austin, McDonald Observatory, Fort Davis, TX 79734, USA*
[9]*INAF – Osservatorio Astronomico di Padova, vicolo dell'Osservatorio 5, I-35122 Padova, Italy*

Accepted 2017 December 12. Received 2017 December 7; in original form 2017 October 3

ABSTRACT

We discuss the self-enrichment scenario by asymptotic giant branch (AGB) stars for the formation of multiple populations in globular clusters (GCs) by analysing data set of giant stars observed in nine Galactic GCs, covering a wide range of metallicities and for which the simultaneous measurements of C, N, O, Mg, Al, and Si are available. To this aim, we calculated six sets of AGB models, with the same chemical composition as the stars belonging to the first generation of each GC. We find that the AGB yields can reproduce the set of observations available, not only in terms of the degree of contamination shown by stars in each GC but, more important, also the observed trend with metallicity, which agrees well with the predictions from AGB evolution modelling. While further observational evidences are required to definitively fix the main actors in the pollution of the interstellar medium from which new generation of stars formed in GCs, the present results confirm that the gas ejected by stars of mass in the range $4\,M_{\odot} \leq M \leq 8\,M_{\odot}$ during the AGB phase share the same chemical patterns traced by stars in GCs.

Key words: stars: abundances – stars: AGB and post-AGB – globular clusters: general.

1 INTRODUCTION

In the last decades the results from high-resolution spectroscopy and space photometry have challenged the traditional paradigma that stars in globular clusters (GCs) are the best example of a simple stellar population (e.g. Gratton, Carretta & Bragaglia 2012; Piotto et al. 2007).

Several studies have outlined that the chemical composition of GC stars, far from being homogeneous, shows well-defined abundance patterns involving the chemical species up to silicon, the most confirmed and investigated being the O–Na anticorrelations (see Gratton et al. 2012, and references therein). The existence of these chemical patterns was observed in all the Galactic GCs studied to date (with the exception of Ruprecht 106; see Villanova et al. 2013), though with clear differences from cluster to cluster (see e.g. Carretta et al. 2009a). The presence of these anomalies in unevolved stars in the main sequence and in the sub-giant branch (Gratton et al. 2001) indicates that these chemical signatures were present in the gas from which the stars formed, ruling out the action of any *in situ* mechanism.

On the photometric side, the discovery of multiple main sequences in the colour–magnitude diagram (CMD) of some GCs (Bedin et al. 2004; Piotto et al. 2007), combined with the analysis of the morphology of the horizontal branch (HB) (D'Antona & Caloi 2004; Caloi & D'Antona 2005, 2007, 2008), leads to the conclusion that part of the stars in GCs were born enriched in helium.

All the aforementioned observational pieces of evidence indicate that star formation in GCs was far from being fully homogeneous, and that after the formation of the first generation (FG) of stars, a

★E-mail: fdellagli@iac.es

second generation (SG) formed[1] from gas which was exposed to proton-capture nucleosynthesis. This opened the way to the search of possible polluters to be active in a self-enrichment mechanism. Because no significant spread is observed in the turn-off region of the CMD of all the GCs observed, the gas from which SG stars formed, processed by internal nucleosynthesis, must have been expelled by FG stars evolving in a time-scale shorter than ∼1 Gyr.

So far four candidates have been proposed: super massive main sequence stars (Denissenkov & Hartwick 2014); fast-rotating massive stars (Krause et al. 2013), massive binaries (De Mink et al. 2009), and massive asymptotic giant branch (AGB) stars (D'Ercole et al. 2010). The problems arising when trying to interpret the observed multiple populations on the basis of the aforementioned scenarios are thoroughly described and discussed in Renzini et al. (2015).

On the way to understand how SG stars formed, an important contribution will be given by data from the Apache Point Observatory Galactic Evolution Experiment (APOGEE; e.g. Majewski et al. 2017), a high-resolution, near-IR, large spectroscopic survey. The APOGEE data allow a good study of the Mg–Al anticorrelation, which is extremely important to discriminate among the possible polluters of the intra-cluster medium from which SG stars formed. This is because the activation of Mg–Al nucleosynthesis is much more sensitive to the temperature than CNO cycling and the Ne–Na chain (Ventura et al. 2013). Moreover, the Mg and Al abundances observed in giant stars definitively reflect their initial chemistry, as there is no way that deep mixing can reach stellar regions touched by magnesium burning.

Mészáros et al. (2015, hereafter ME15) presented APOGEE data for 10 GCs, spanning a range of metallicity from [Fe/H] = −2.37 to [Fe/H] = −0.78. For the stars in all 10 clusters the surface abundances, when possible, of the elements involved in CNO cycling and Mg–Al–Si nucleosynthesis were measured.

A first attempt to interpret ME15 data was made by Ventura et al. (2016), focusing on only five of the GCs in the ME15 sample: the main conclusion reached by Ventura et al. (2016) is that the extent of the Mg–Al and Mg–Si anticorrelations observed, particularly the variation with the metallicity, could be explained by hypothesizing that SG stars formed from gas lost by stars of mass in the range 4–8 $M_{\odot}$ during the AGB phase.

In this paper we make a step forward, by considering 9 out of 10 of the GCs studied by ME15 (we skipped NGC 5466 where only eight stars were observed), attempting to infer their star formation history after the formation of the FG. While the analysis by Ventura et al. (2016) is limited to the Mg, Al, Si, and O abundances, here we consider also the carbon and nitrogen data, being aware that the surface mass fractions of these elements are subject to a significant alteration during the RGB ascending. Furthermore, while Ventura et al. (2016) used pre-existing AGB models with a chemistry similar to the stars in the ME15 sample, here we use updated AGB models, calculated specifically for the present analysis, where the initial chemical composition is assumed ad hoc to be the same as derived from ME15 for the FG stars of the different clusters. This is extremely important, as the interpretation of the results does not rely on any artificial scaling of the abundances, which may partly alter the results obtained.

[1] Here we refer generally with SG to all the stars formed after the FG, despite in some GCs it was confirmed that more than two groups of stars exist, differing in their chemical composition.

In this study we focus on the interpretation of the high-resolution spectroscopic data based on the yields from massive AGB stars, without entering into the dynamical details of the self-enrichment process. All the arguments related to the modality with which SG stars formed (D'Ercole et al. 2008), the difference in the spatial distributions of FG and SG stars, which makes the former more exposed to escape from the cluster (Vesperini et al. 2013), the need for dilution with pristine gas (D'Ercole, D'Antona & Vesperini 2011), the possibility that part of the pristine gas survives to the epoch of type II SNe explosions (D'Ercole, D'Antona & Vesperini 2016), are thoroughly documented in the literature and will not be addressed here. Our aim is to answer the following question: can the large data set presented by ME15 be explained on the chemical side within the context of the self-enrichment scenario by AGB stars?

To this goal, we study the ME15 GCs individually, doing a detailed comparison between the data set and the chemistry of the AGB ejecta. The main scope is to deduce the origin of SG stars and whether the formation of SG occurred from the pure AGB ejecta or if some dilution with pristine gas in the cluster is required. Whenever possible, we confront our conclusions with results from photometry, as the latter provides valuable information on the helium spread of the clusters stars, a key indicator of the existence and of the degree of contamination of SG stars compared to their FG counterparts.

The paper is organized as follows: Section 2 contains an overview of the physical input for the AGB models adopted and the main chemical points regarding their ejecta; Section 3 is devoted to the analysis of the data for each GC, via a detailed comparison with the yields from the AGB stars with the same chemical composition; in Section 4 we extend our comparison to the O–Na plane; a general discussion of the results obtained is presented in Section 5, whereas the conclusions are given in Section 6.

2 MASSIVE AGBS MODELS: NUCLEOSYNTHESIS AND YIELDS

The AGB models used here have been calculated specifically for the present investigation. They were computed by means of the ATON code for the stellar evolution. The interested reader can find in Ventura et al. (1998) a detailed description of the numerical structure of the code; the most recent updates are given, e.g. in Ventura & D'Antona (2009).

2.1 The initial chemistry

To choose the O, Mg, Al, and Si initial chemical composition of the models used to study each individual cluster, we relied on the assumed chemistry of FG stars, reported in Table 7 of ME15, where they summarize the average FG abundances of each cluster. Clusters similar in metallicity and in the O, Mg, Al, and Si abundances were grouped together, and studied by means of a unique set of models. The mass fractions of the other species were scaled according to the overall metallicity and the solar distribution by Lodders et al. (2003). This choice also includes C and N, for which we assumed [C/Fe] = [N/Fe] = 0. Note that, because of the effects of the first dredge-up (FDU) and non conventional mixing (see e.g. Charbonnel & Lagarde 2010), the surface abundance of C and N in RGB stars is not expected to reflect the composition of the gas from which the stars formed.

The overall theoretical framework consists in six sets of AGB models, with mass in the range 4–8 $M_{\odot}$, whose initial chemical composition is reported in Table 1.

Table 1. The chemical composition assumed to calculate the AGB models used to study the GCs in ME15 sample. The metallicity and the mass fraction of the individual species have been taken from ME15. The only exceptions are C and N, for which a solar-scaled abundance was adopted in all cases.

cluster	[Fe/H]	Z	Y	[C/Fe]	[N/Fe]	[O/Fe]	[Mg/Fe]	[Al/Fe]	[Si/Fe]
M92, M15	− 2.3	2×10^{-4}	0.25	0.0	0.0	0.65	0.30	− 0.20	0.40
M53	− 2.0	4×10^{-4}	0.25	0.0	0.0	0.60	0.40	− 0.10	0.40
M13, M2, M3	− 1.5	10^{-3}	0.25	0.0	0.0	0.55	0.20	0.00	0.40
M5	− 1.3	1.5×10^{-3}	0.25	0.0	0.0	0.40	0.25	0.00	0.35
M107	− 1.0	2.5×10^{-3}	0.25	0.0	0.0	0.40	0.35	0.50	0.50
M71	− 0.8	6×10^{-3}	0.26	0.0	0.0	0.50	0.45	0.45	0.40

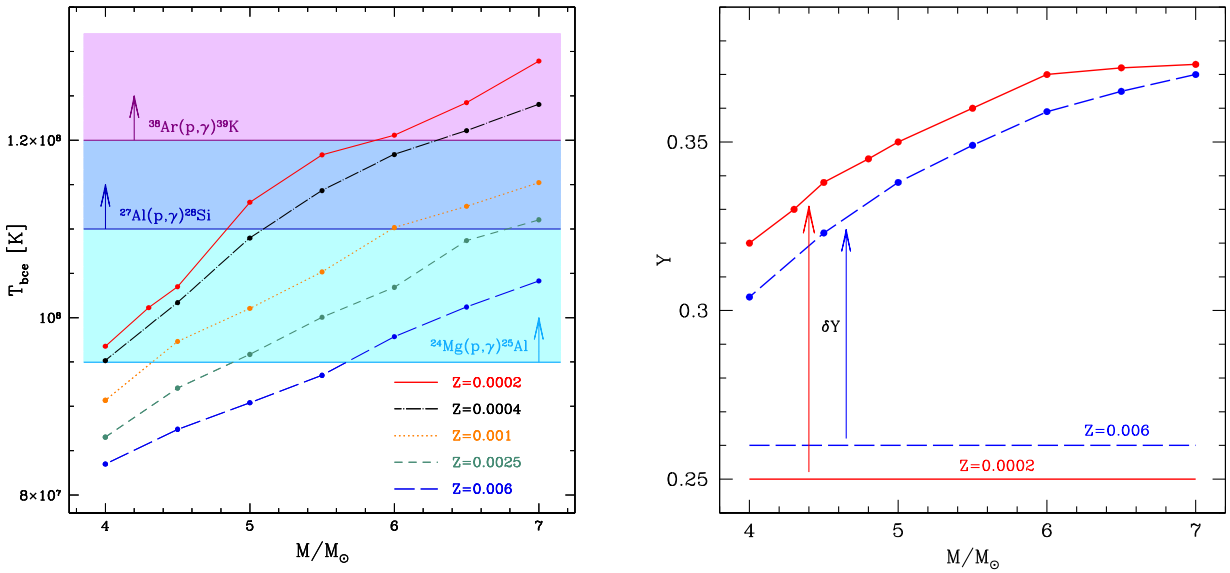

Figure 1. Left: typical temperature at the base of the convective envelope during the AGB phase, as a function of the initial mass of the star at different metallicities. The temperatures above which some important nuclear reactions (labelled) are efficient are shown as horizontal lines and correspondent shaded area. Right: helium yields as a function of stellar masses for the highest ($Z = 6 \times 10^{-3}$, solid-red line) and lowest ($Z = 2 \times 10^{-4}$, dashed-blue line) metallicity considered in this work. The horizontal lines at Y=0.26 and Y=0.25 represent the initial helium content considered respectively.

2.2 HBB in massive AGB stars

The evolution of stars during the AGB phase is thoroughly documented in the literature. The reviews by Herwig (2005) and Karakas & Lattanzio (2014) present an exhaustive description of the physical and chemical evolution of these stars, and a discussion of how the uncertainties regarding some of the physical ingredients adopted affect the results obtained.

For what attains the stars of interest here, we know that the AGB evolution of $M \geq 4$ M$_\odot$ stars is characterized by the ignition of the so-called hot bottom burning (hereinafter HBB). HBB consists in the ignition of a series of proton capture reactions at the base of the convective mantle, taking place when the temperature in those regions of the stars, $T_{\rm bce}$, exceeds ∼30 MK (Renzini & Voli 1981; Blöcker & Schöenberner 1991). The activation of HBB, due to a partial overlapping of the convective envelope with the CNO burning shell, requires core masses above ∼0.75 M$_\odot$, corresponding to initial masses above ∼4 M$_\odot$ (Ventura et al. 2013).

When HBB is active, the gas ejected by the stars will show the imprinting of the nucleosynthesis experienced at the base of the convective envelope, because convective currents are extremely efficient in homogenizing the whole external mantle, up to the outermost layers, which are gradually lost via stellar winds.

Common features of all the stars experiencing HBB are the destruction of the surface C and the synthesis of great amounts of N, a process which requires $T_{\rm bce} \sim 30$ MK. The possibility that more advanced proton captures are activated depends primarily on the values reached by $T_{\rm bce}$.

The left-hand panel of Fig. 1 shows the values of the temperatures at the base of the envelope of the AGB models used in the present analysis,[2] for different masses and metallicities. Two general trends are evident from the figure: (a) for a given chemical composition, higher masses evolve at larger temperatures, due to their higher core masses; (b) lower metallicity AGB stars achieve higher $T_{\rm bce}$.

In the left-hand panel of Fig. 1 we also show the threshold temperatures above which different proton-capture channels are activated. This information is crucial to understand the kind of pollution expected from these objects and how advanced the proton-capture nucleosynthesis experienced will be. While we will discuss in detail the various yields in the following sections, a clear result shown

[2] The temperature at the base of the surface convection region increases in the early AGB phases and decreases in the final stages, after most of the envelope was lost by stellar winds. However, for most of the time during which mass loss occurs, the temperature keeps approximately constant, thus allowing us to provide a typical value.

in Fig. 1 is that the most advanced nuclear channels, in particular the ignition of Mg–Al–Si nucleosynthesis, can be achieved only in the most metal-poor AGB stars.

We believe important to mention at this point that while the trend of the HBB temperature with mass and metallicity, shown in the left-hand panel of Fig. 1, can be considered general, i.e. independent of the details of AGB modelling, the strength of HBB experienced, hence the temperatures reached by the base of the convective mantle, depend on the treatment of convection, particularly on the way that the temperature gradient is calculated in regions unstable to convective motions. In the analysis by Ventura & D'Antona (2005), it is shown that the use of the Full Spectrum of Turbulence (FST; Canuto & Mazzitelli 1991) to model convection leads to strong HBB, with large temperatures at the base of the envelope. Conversely, the use of the classic Mixing Length Theory (MLT), particularly when the standard calibration used to fit the evolution of the Sun is adopted, determines much weaker HBB conditions. The AGB models used in this work are based on the FST description, which has the advantage that the results obtained in this context are independent of any calibration of free parameters. When the MLT model is used, the situation is more complex, because the results are sensitive to the choice of the free parameter α, giving the mixing length. When the solar-calibrated MLT α is adopted, the degree of the nucleosynthesis experienced is much lower than that in the FST case, because the temperatures are below 10^8 K, even in low-metallicity massive AGB stars (e.g. Cristallo et al. 2015).

Thus, in the MLT case there is no way that the AGB yields can reproduce the observed O–Mg–Al–Si chemical patterns. The use of a higher α leads to a more advanced HBB nucleosynthesis; although only in the most metal-poor stars with mass close to the threshold for the core collapse, the temperatures become high enough to efficiently activate magnesium burning (e.g. Fishlock et al. 2014).

2.3 AGB stars as helium manufacturers

An important point in the pollution by massive AGB stars is that the gas expelled by these objects is enriched in helium. This is shown in the right-hand panel of Fig. 1, where we show the average helium abundance of the gas ejected as a function of stellar masses for the highest ($Z = 6 \times 10^{-3}$) and lowest ($Z = 2 \times 10^{-4}$) metallicity considered in this work. While the temperatures at the base of the envelope, that reflects into the degree of the nucleosynthesis experienced, display an extreme sensitivity to the metallicity, the helium in the ejecta is mainly determined by the initial mass of the star. This is because most of the surface helium enrichment occurs during the second dredge-up following the core He-burning phase, and is primarily determined by the extent of the inwards penetration of the convective envelope down to regions previously touched by CNO activity: the efficiency of this process is related to the mass of the envelope and is scarcely affected by the chemical composition of the star (Ventura 2010; Karakas & Lattanzio 2014). The second dredge-up provokes a rise in the surface helium, which increases with the mass of the star, ranging from $\delta Y \sim 0.02$, for $M = 4\,M_\odot$, to $\delta Y \sim 0.12$, for $M = 8\,M_\odot$.

Based on the results shown in right-hand panel of Fig. 1, we understand that if the formation of SG stars in GCs is determined by the AGB ejecta, these stars must be enriched in helium. The extent of such enrichment depends on the range of masses involved in the pollution of the interstellar medium and on the degree of dilution of the AGB gas with pristine matter in the cluster. If no dilution occurred, SG stars will definitively show evidences of helium enrichment, which leaves an important signature in the distribution of the stars on the MS (Piotto et al. 2007) and in the morphology of the HB (D'Antona et al. 2002). The most extreme case is when the formation of SG stars occurs within ∼10–20 Myr after the type II SNe explosions epoch, directly from the winds of the most massive ($M \sim 7$–$8\,M_\odot$) AGB stars, without dilution with pristine gas. In this case, a high-helium stellar component would be present in the cluster, which would define a blue-hook structure on the HB. This is the scenario invoked by D'Antona & Caloi (2004) to explain the bluest stars in the HB of NGC 2808 and by Di Criscienzo et al. (2011) to account for the 'blue hook component of the HB of NGC 2419.

3 RESULTS

3.1 The low metallicity clusters: M15 and M92

M15 and M92 are the most metal poor clusters in the ME15 sample, with [Fe/H] ~ -2.3, which corresponds to a metallicity $Z = 2 \times 10^{-4}$. Fig. 1 shows that a very advanced HBB nucleosynthesis is expected to occur in AGB models of this chemical composition, because all the stars with mass $M > 4.3\,M_\odot$ reach temperatures at the base of the envelope exceeding 100 MK.

Figs 2 and 3 show the abundances of the ejecta of $Z = 2 \times 10^{-4}$ AGB models (red squares) in different planes. The high HBB temperatures given above trigger a significant depletion of Mg into Al. From the figures we see that Mg depletion reaches δ[Mg/Fe] ~ -0.6 whereas the increase in aluminium is δ[Al/Fe] ~ 1. The HBB temperatures at these low metallicities are so hot that part of the aluminium produced is converted into silicon (see Fig. 1). The reason for the negative trend with mass of the aluminium content of the ejecta is that higher mass models are exposed to a more efficient Al burning, as confirmed by the increase in the silicon content, shown in the top, right-hand panels of Figs 2 and 3.

These extremely high temperatures certainly imply also a very advanced CNO cycling. Indeed, Figs 2 and 3 show that the AGB ejecta are oxygen-poor (δ[O/Fe] ~ -1.1). At the same time the gas from these stars is strongly enriched in N, which has an enhancement factor[3] in the range 50–200. The ejecta are not carbon poor, despite the high rates of carbon burning reactions. This is because at these extremely low metallicities even a small number of third dredge-up events are sufficient to increase significantly the surface carbon. Since part of this carbon is converted into nitrogen by HBB, this same reason explains the extremely large nitrogen abundances.

Figs 2 and 3 show the observations of M15 and M92 by ME15 (black dots) overlapped to the models. The blue regions identify the area between the dilution curves for AGB stars of 4.5 and 5.5 solar masses, obtained by mixing different fractions of the ejecta of AGB stars with pristine gas, sharing the same chemical composition of FG stars (reported in Table 1). When a sufficient number of data are available, to compare the theoretical dilution pattern with the one traced by the data, we have used the following equation:

$$[X] = \log[(1 - dil)10^{[X]_{FG}} + dil\,10^{[X]_{SG}}] \quad (1)$$

where [X] is the logarithmic abundance of a given element. $[X]_{FG}$ and $[X]_{SG}$ are, respectively, the abundances of the pristine gas and processed material; *dil* represents the fraction of pristine gas in the

[3] We use the standard definition of 'enhancement factor', as the ratio between the average abundance of a given chemical species in the ejecta and the initial mass fraction.

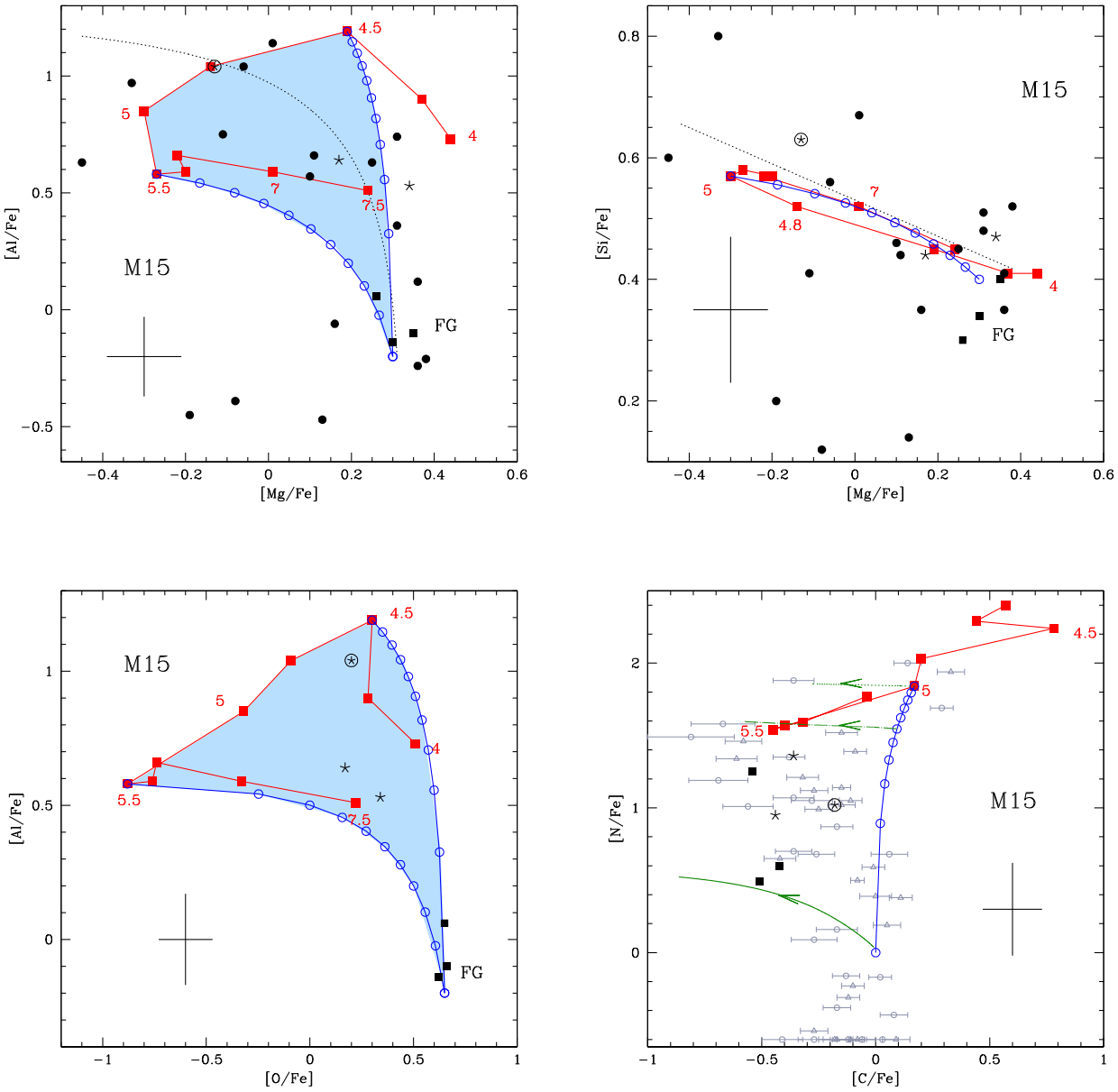

Figure 2. M15 stars from ME15 are shown as full dots in the Mg–Al (top-left) and Mg–Si (top-right). CNO abundances are measured for part of the sample. They are identified by black squares, stars, and stars surrounded by open circles according to the anticorrelation pattern (low, intermediate, and high, respectively) shown in the O–Al (bottom-left) and C–N (bottom-right) planes. The black crosses indicate typical APOGEE error bars. Results from the fits are shown with dotted lines. Data sets from Cohen, Briley & Stetson (2005a) are shown with grey, open triangles ($T_{\rm eff} < 5300$ K) and circles ($T_{\rm eff} > 5300$ K), in the C–N plane. The yields of AGB models of metallicity $Z = 2 \times 10^{-4}$ are indicated with red squares; the numbers close to the squares indicate the initial masses. Blue, open circles indicate the chemistry expected from mixing of the AGB ejecta with pristine gas, with percentages of the latter ranging from 0 to 100 per cent, in steps of 10 per cent. The points corresponding to 100 per cent dilution are close to the FG label. Green curves represent the evolution of a 0.9 $M_{\odot}$ star, currently evolving through the RGB. Three initial chemical compositions are considered: the chemistry of FG stars (solid), the chemistry of pure AGB ejecta (dotted), and of a 50 per cent mix of pristine matter with AGB gas (dashed-dotted).

gas where second generation formed. In order to obtain the data pattern, for $[X]_{FG}$ we assume the average values of [Mg/Fe] and [Al/Fe] for the FG reported in Table 7 by ME15; for $[X]_{SG}$ we assume the minimum value of magnesium observed and we derive the SG aluminium value by minimizing the root mean square (rms) of the residuals along the fitting relations. In the case of M15 in Fig. 2 we obtain $[Al/Fe]_{SG} = 1.18 \pm 0.05$ with rms = 0.46, while for M92 we find $[Al/Fe]_{SG} = 0.85 \pm 0.06$ with rms = 0.47. The same procedure is adopted in the O–Al plane, for all the GCs where a sufficient number of stars are available.

We caution the reader since the beginning regarding the fact that the interpretation of the observations in the C–N plane is trickier than others. This is because the abundances of C and N are altered during the RGB ascending, due to deep mixing. While 'standard' evolution theories[4] for the FDU predict a C depletion of ∼20–30 per cent, several observational evidences (e.g. Gratton, Sneden

[4] We indicate with 'standard the results obtained when the border of the convective regions is fixed via the Schwartzschild criterion.

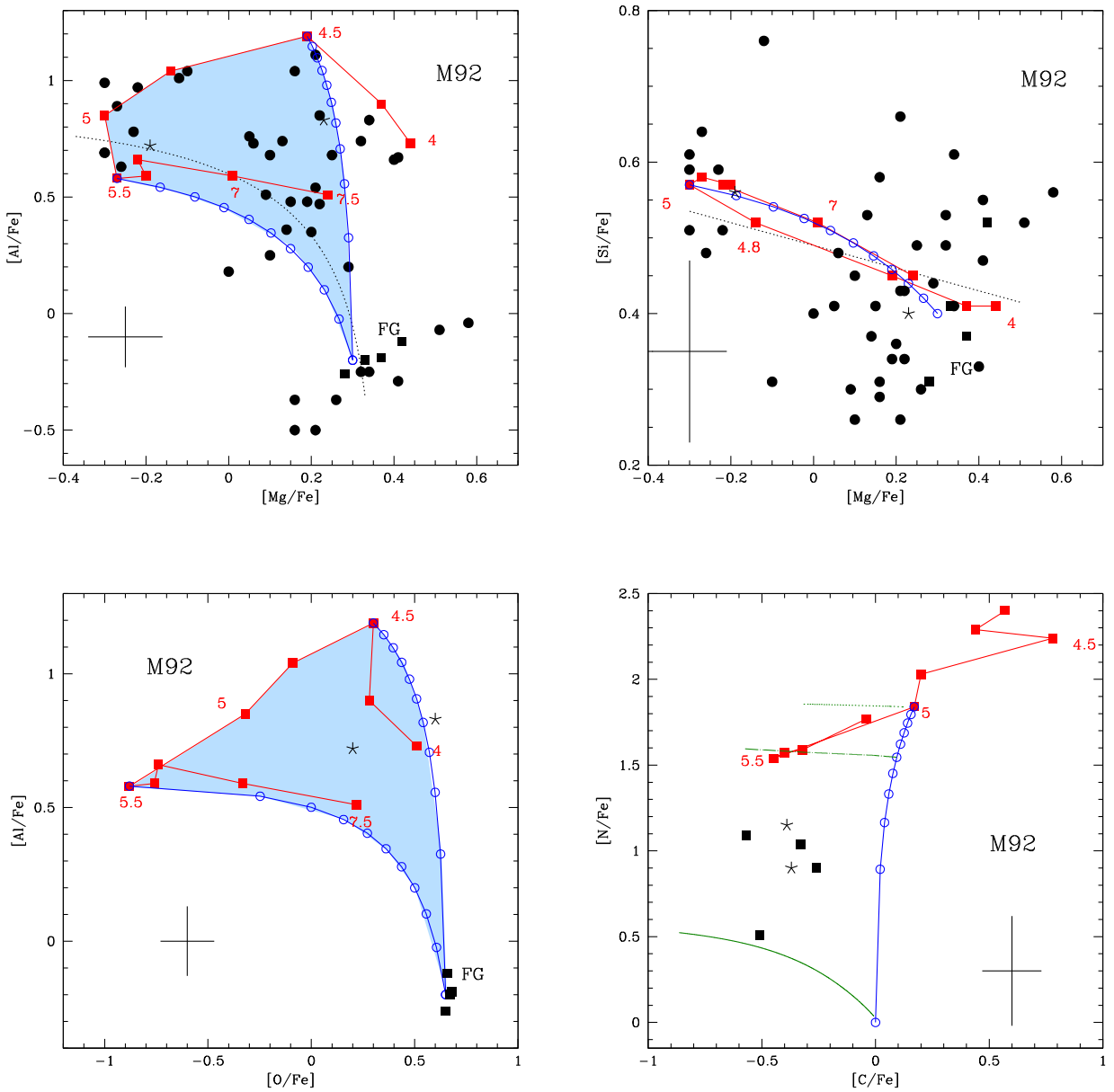

Figure 3. M92 stars from ME15 are shown in the same planes and with the same symbols as in Fig. 2. They are compared with the yields of AGB models of the same metallicity ($Z = 2 \times 10^{-4}$) as in the case of M15.

& Carretta 2004) suggest a deeper mixing in the post-bump phases, likely associated with thermohaline mixing (Charbonnel & Lagarde 2010). Therefore, the C and N abundances of the giant stars do not reflect the initial chemistry.

To quantify this effect in the comparison with the observations, we calculated stellar models evolving through the RGB in which deep mixing is applied after the luminosity bump, with the same extent required to reproduce results from thermohaline mixing models. We assumed a typical mass currently evolving through the RGB ($0.9\,M_{\odot}$). Starting from the chemical composition discussed in this section, we compute the evolution adopting three chemical compositions. They correspond to the chemistry of FG stars (pure pristine gas), of a 50 per cent mix of pristine matter with AGB gas and of a pure AGB ejecta. The results are indicated with green curves, respectively, with solid, dotted-dashed, and dotted lines in Figs 2 and 3. We note that in all cases the surface carbon decreases during the RGB evolution, because of mixing surface matter with C-poor matter exposed to CNO processing. On the other hand, the surface N of the models with chemistry polluted by AGB gas remains unchanged, because the initial N is higher than the equilibrium abundances expected in regions exposed to CNO cycling. We did the same computation at higher metallicity ($Z = 2.5 \times 10^{-3}$) and we found that similar spread is predicted: δ([C/Fe]) varies from $\sim$0.7 dex in the case of a pure gas pristine initial chemistry, to $\sim$0.5 dex in the 100 per cent AGB ejecta. Spread in N is found only in the first case [δ([N/Fe] $\sim$ 0.6)], for the same reasons previously stated. Therefore, we generally conclude that detailed N measurements can be a valuable indicators of the degree of dilution of the contaminating gas with pristine matter in the metallicity range here considered. Due to known errors in the ASPCAP

determination of the main stellar parameters (e.g. Teff, logg), which affect the derived abundances (including [C,N,O/Fe]) of SG stars in GCs (Jonsson et al., in preparation), ME15 chose to derive abundances independent of ASPCAP, using photometric temperatures and gravities. The abundances derived by ME15 do not exhibit the systematic errors that ASPCAP do. Nevertheless, [N/Fe], together with [C/Fe], are still affected by high level of uncertainty due to the fact that CN and CO lines are often blended with other molecular or atomic lines. This affects low-metallicity measurements in particular ([Fe/H] ≤ -2), as the CO, OH, and CN lines are extremely weak in this parameter region; therefore, it is not possible to give more information than upper and lower limits in this range of metallicities. This is clearly reported by ME15 where [N/Fe] and [C/Fe] errors are relatively high ($\pm 0.1 - 0.32$).[5] We take into account all these points in the following discussion and to draw any conclusion from this analysis.

3.1.1 M15

For this cluster we mainly base our analysis on the Mg–Al–Si abundances, because the abundances of the CNO elements are available for only a few stars. In the comparisons, we do not consider the three outlier stars,[6] showing very low Al ([Al/Fe] ~ -0.5) and Si ([Si/Fe] ≤ 0.2) abundances, with [Mg/Fe] in the range $-0.2 <$ [Mg/Fe] $< +0.15$.

In the Mg–Al plane, shown in the top-left panel of Fig. 2, we can clearly distinguish an anticorrelation pattern, the stars with most extreme chemical composition (Mg-poor/ Al-rich), in the left, upper region of the plane, showing up an overall magnesium depletion with respect to the FG of $\sim$0.6 dex, and an Al enhancement of $\sim+$ 1.4 dex. As shown in the figure, the yields of AGB stars show the same Mg and Al spread observed. These results suggest that these stars formed from the ejecta of 4.5–6 solar masses AGBs, with only a $\sim$10 per cent contribution from pristine gas.

Some stars, which fall within the blue region, are characterized by a chemical composition somewhat intermediate between the FG and the stars with the most extreme chemical composition: these are SG stars, formed from AGB ejecta diluted with $\sim$40–50 per cent of pristine gas of the cluster.

In the Mg–Si plane, the data indicate the presence of a silicon spread,[7] δ[Si/Fe] $\sim +0.2$ dex, which indicates that the material from which the Mg-poor and Si-enhanced stars formed was exposed to Al-burning. The observed silicon spread is consistent with what is expected from the yields as shown in the top-right panel of Fig. 2. While the distinction between FG and SG stars is more clear in the Mg–Al panel discussed previously, here we stress the importance of the existence of an Si spread, because Si production requires hotter temperatures than those for Al, above $\sim$100 MK, thus providing important hints on the class of polluters which contaminated the intra-cluster medium.

The CNO abundances are available only for six stars in the sample. Three of them do not show any Al enhancement or O and Mg depletion, which suggests that they belong to the FG of the cluster; these stars have been indicated as full squares in Fig. 2. The three stars left show the imprinting of Mg and O depletion and Al enhancement, thus they belong to the SG. Two of these stars, indicated with asterisks, show a chemical composition intermediate between FG and SG stars, thus they formed from dilution of AGB gas with pristine matter. One out of the six stars (2M21291235+1210498) indicated with an asterisk surrounded by a circle, shows up a significant enhancement of aluminium (above 1 dex), and a magnesium content $\sim$3 times smaller than FG stars, a trace of a more extreme chemical composition. Interestingly, the combination of the Mg, Al, and O abundances for this star reflect the chemical composition of the ejecta from AGB stars of mass 4.5–5 $M_{\odot}$.

As stated above, any further conclusion based on the comparison between the present data set and the models in the C–N plane is not straightforward, in particular in the lower metallicity cases and with such a small sample of stars. In the case of M15, nonetheless, we may take advantage of the comparison with the results by Cohen et al. (2005a), who measured the C–N abundances of a wide number of RGB stars, shown in the bottom-right panel of Fig. 2. The wide spread of $\sim$1 dex observed in [N/Fe] is in agreement with the prediction of the models. Cohen et al. (2005a) sampled the entire RGB, including stars below the bump, thus not exposed to any deep-mixing. We indicate these sources according to their estimated temperature in order to distinguish stars below (circles, $T_{\rm eff} > 5300$ K) and above (triangle, $T_{\rm eff} < 5300$ K) the location of the FDU. It is interesting to discuss the first group of stars: part of them show [N/Fe]$\sim$0, without carbon depletion, clearly indicating the pure initial chemistry of the FG, not affected by any mixing episodes. On the other hand, in the same class of stars we can identify the SG, on the basis of their higher nitrogen abundances, associated with a progressively increasing carbon depletion. This reflects the imprinting of the medium where they formed, in remarkable agreement with the predictions from the AGB yields.

To summarize, ME15 data indicate that M15 harbours SG stars, formed from nuclearly processed gas, which is consistent with the AGB self-enrichment expectations. The presence of SG stars in M15 is not new, as evidence for the presence of SG stars in this cluster dates back to the work by Cohen et al. (2005a). The UVES data by Carretta et al. (2009b) also suggest that SG stars exist in M15: the observations outline the presence of an O–Na anticorrelation trend (see Section 4), although a solid interpretation of this result is partly disturbed by the fact that for most stars only upper limits exist for the oxygen abundances. More recently, Milone et al. (2017), based on high-precision photometry of RGB stars, estimated that 60 per cent of the stars in M15 belong to the SG. The presence of SG stars could also explain the helium spread invoked to account for the morphology of the HB: VandenBerg, Denissenkov & Catelan (2016) claim that helium mass fractions $Y > 0.29$ are required to reproduce the blue part of the HB of M15, whereas Milone et al. (2014) conclude that a helium spread $\delta Y \sim 0.07$ would be compatible with the distribution of M15 stars on the HB. Interestingly, such large spread would imply the existence of stars formed with $Y \sim 0.32$, the helium obtained when diluting pure AGB ejecta with $\sim$20 per cent of pristine gas; this is in agreement with our interpretation of M15 SG stars with the most extreme chemistry.

[5] Note that these errors do not include possible systematic/random effects due to the methodology employed in the chemical abundances derivation (the use of spectral windows versus the entire spectrum, model atmospheres, linelists, etc.)

[6] These stars show a peculiar chemical composition very different from the rest of cluster stars, while they do not show stellar parameters and radial velocities so different to the rest of the cluster stars. We believe that the ME15 methodology for the derivation of their chemical abundances, or the DR10 data reduction pipeline has failed with these stars for some unknown technical reasons.

[7] This is confirmed by the application of the least square fit method to the data, from which we obtain a straight line with a steepness of -0.3 and a scatter of 0.09.

3.1.2 M92

On the chemical side, M92 is extremely similar to M15, in terms of metallicity and of the Mg–Al–Si content of FG stars. For these elements a deeper analysis is possible compared to M15, because more data are available, while the CNO elements are available for six stars only. The comparison between the observations and $Z = 2 \times 10^{-4}$ models are shown in Fig. 3, with the dilution curves obtained by mixing gas from AGB stars with variable percentage of pristine matter.

Similarly to M15, the Mg–Al plane proves the best locus to draw information on the formation of SG stars, owing to the small increase expected for silicon and the paucity of data available for CNO elements. The most extreme chemistries of M92 stars correspond to an overall Mg decrease of ∼0.6 dex and an ∼1.3 dex of increase in Al, with respect to the average abundances of the FG stars; same abundances are expected from the AGB ejecta.

These results confirm on qualitative grounds the conclusions drawn by Ventura et al. (2016) regarding the distribution of M92 giants in the Mg–Al plane. Compared to Ventura et al. (2016), here we obtain a better agreement between data and theoretical predictions, because in this case we used the same Mg abundance of FG stars, namely [Mg/Fe] = +0.3, 0.1 dex smaller than in Ventura et al. (2016): this is the reason for the smaller Mg and Al contents in the ejecta of AGBs, which nicely fit the data shown in the left, bottom panel of Fig. 3.

Compared to M15, we note that the data cover the Mg–Al plane more uniformly, suggesting a formation of the SG with different degrees of dilution with pristine gas of the cluster. However, we cannot draw conclusions on any difference in the formation of the SG in the two clusters, as the dissimilarity between the two clusters could be due to the smaller data set available for M15.

The Mg–Si anticorrelation is more evident in M15 than in M92[8] due to the high Si dispersion of the data around [Mg/Fe] ∼ 0.2. On the other hand, stars with the lowest magnesium ([Mg/Fe] < −0.1) show up a silicon content [Si/Fe] > 0.45; this is in good agreement with the prediction from yields of AGB stars, suggesting that these stars possibly formed from gas with a very limited (if any) degree of dilution with pristine matter.

Turning to the O-Al plane (see the left-hand, bottom panel of Fig. 3), we find that four out of the six stars for which oxygen data are available belong to the FG. These stars, indicated with full squares, exhibit a rather homogenous Al content; their position in the two planes discussed previously confirms this interpretation. The other two stars (asterisks) for which CNO data are available are more Al-rich, one of them with a Mg and O contents significantly smaller than FG stars: from their surface chemistry we interpret them as belonging to the SG of the cluster, formed from AGB gas diluted with ∼20 per cent (the one with the smallest Mg, 2M17163748+4306155) and ∼50 per cent (2M17171307+4309483) of pristine material. While the same reasons stated for M15 (limits in the determination of the abundances in the low metallicity range, a limited number of stars, etc.) prevents a clear interpretation of the C–N plane, in the right-hand, bottom panel of Fig. 3, we display the results of the AGB ejecta and stellar evolution calculations with deep mixing.

In conclusion, the analysis of the wide Mg-Al anticorrelation measured provide a strong indication of the presence of an SG in M92, formed from gas which was exposed to advanced proton-capture nucleosynthesis. Milone et al. (2017) conclude that the FG stars account for ∼30 per cent of the whole population of M92, a result consistent with our understanding of the Mg–Al data (see the left-upper panel of Fig. 3). The comparison of the data points and the chemistry of AGB ejecta in the Mg–Al and Mg–Si planes suggests that M92 hosts a few stars with a very extreme chemical composition, formed by pure AGB gas, possibly mixed with a very tiny percentage of pristine matter. These stars, which would have a helium content $Y \geq 0.30$ (see the right-hand panel of Fig. 1), apparently have no counterparts on the HB of M92, according to the analysis by VandenBerg et al. (2016), who claim that a very small helium spread is required to reproduce the morphology of the HB of this cluster.

3.2 M53: a cluster at the edge

The metallicity of this cluster is higher ([Fe/H] = −1.96) than M15 and M92. Magnesium, aluminium, and silicon abundances have been measured for 16 stars, for 6 of which the CNO values are available. The models used to study M53 have been calculated with metallicity $Z = 4 \times 10^{-4}$. The comparison between the data and the models is reported in Fig. 4.

The extents of Mg-depletion and Al-enhancement observed in this cluster and shown in the top-right panel of Fig. 4 are δ[Mg/Fe] ∼ −0.2 dex and δ[Al/Fe] ∼ +1.2 dex, respectively. These numbers are in good agreement with the AGB models shown here. In the same panel of this figure, the result of the fitting procedure for M53 is shown, obtaining $[Al/Fe]_{SG} = 0.86 \pm 0.06$ with rms = 0.34.

Compared to M15 and M92, the Mg-depletion is significantly reduced, whereas the abundances of the most Al-rich stars are comparable. These differences can be understood on the basis of the lower HBB temperatures of the intermediate mass stars that evolved in M53, compared to M15 and M92. Based on the discussion in Section 2.2 and on the results shown in Fig. 1, we know that the HBB experienced at the base of the convective envelope is stronger the lower is the metallicity. The Al-enhancement, as shown by the data and the models, is rather independent of Z in this metallicity domain, unlike the depletion of magnesium. This reflects the difference in the nucleosynthesis experienced by the two chemical species under the effects of HBB. Magnesium is destroyed during the whole AGB phase, the depletion rate being larger the higher is T_{bce}. Al is subject to both a creation path and a destruction channel, the latter leading to the production of silicon. It is not surprising that the amount of Al produced is almost independent of Z: as far as the HBB temperatures exceed ∼110 MK, it is expected that silicon production occurs (see Fig. 1), with a partial depletion of the Al previously synthesized by Mg burning (an exhaustive discussion on the Mg–Al–Si nucleosynthesis can be found in Arnould, Goriely & Jorissen 1999).

The maximum silicon spread expected from the AGB ejecta is δ[Si/Fe] < 0.1 dex in the case of M53. This is because the metallicity of this cluster is sufficiently low for the FG stars of intermediate mass to have produced Mg-poor and Al-rich gas, but at the same time it is high enough to avoid a more advanced HBB nucleosynthesis, required to eject gas enriched in silicon. For this reason we do not expect any Si-enhancement for higher metallicities GCs and we consider M53 as an edge point in this excursion. The silicon spread expected is smaller than the dispersion and the typical error of the data is shown in the right, top panel of Fig. 4. It makes really hard to confirm or disproof the presence of Mg–Si anticorrelation in

[8] The least square fitting of the data provides a steepness of −0.15 and a scatter of 0.1.

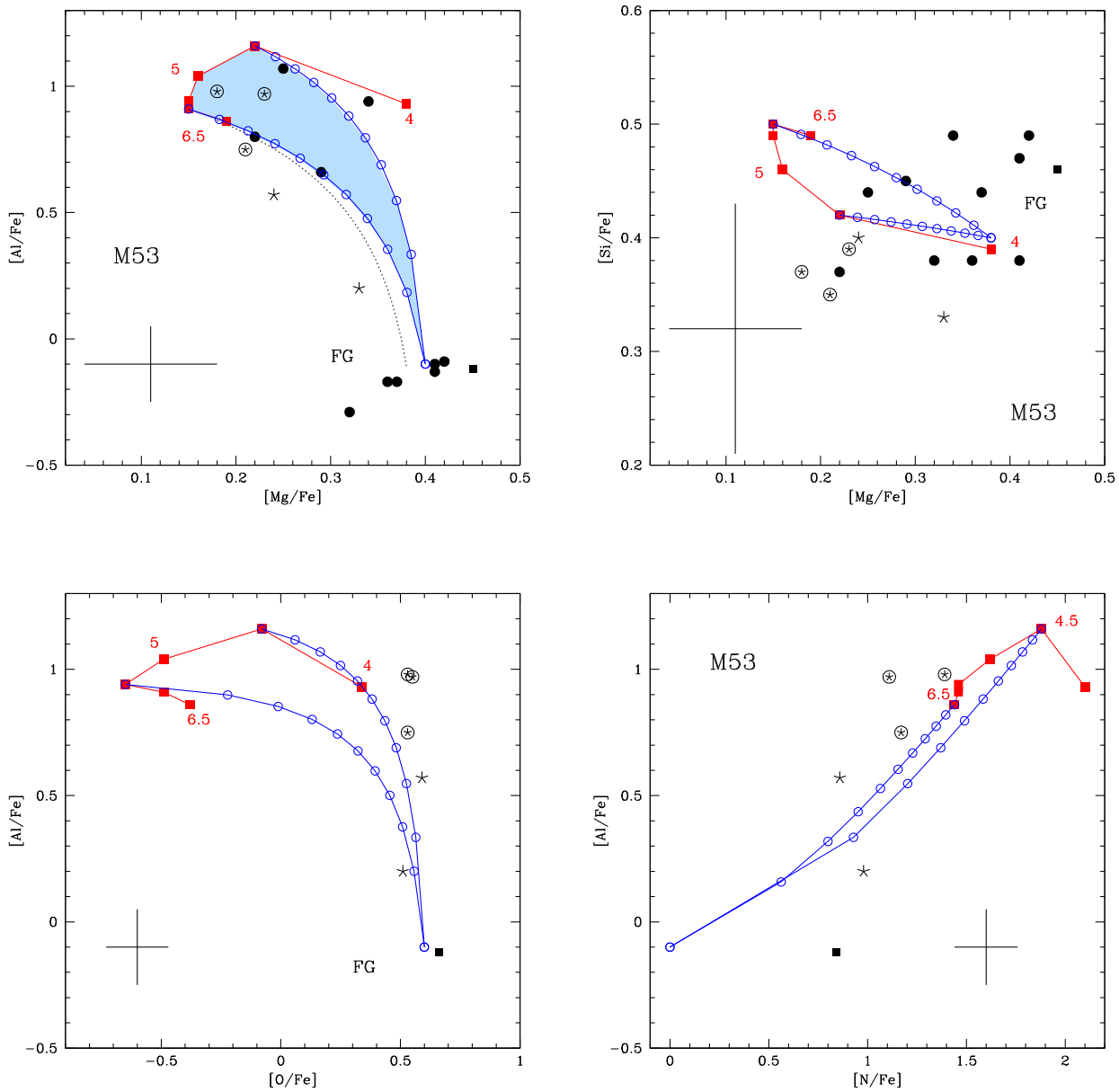

Figure 4. M53 stars from ME15 are shown as full dots in the Mg–Al (top-left) and Mg–Si (top-right). CNO abundances are measured for part of the sample. They are identified by black squares, stars, and stars surrounded by open circles according to the anticorrelation pattern (low, intermediate, and high, respectively) shown in the O–Al (bottom-left) and N–Al (bottom-right) planes. Results from the fits are shown with dotted lines and the black crosses indicate typical error bars. The yields of AGB models of metallicity $Z = 4 \times 10^{-4}$ are indicated with red squares; the numbers close to the squares indicate the initial masses. Blue, open circles indicate the chemistry expected from mixing of the AGB ejecta with pristine gas, with percentages of the latter ranging from 0 to 100 per cent, in steps of 10 per cent. The points corresponding to 100 per cent dilution are close to the FG label.

this cluster. More precise measurements and larger sample of data would be useful to draw any conclusion in this regard and on the duration of the formation of the SG observed in the Mg–Al plane.

In the O–Al plane we base our analysis on the six stars for which the oxygen is available. One star (2M13123617+1807320), indicated with a full square, shows a typical FG chemistry, based on the O, Mg, and Al abundances. The five stars left show the presence of some Al-enrichment, suggesting pollution from gas exposed to nuclear activity. For two out of the five stars the aluminium abundance observed is [Al/Fe] $< +0.5$ (shown with asterisks in Fig. 4), which suggests significant (> 50 per cent) dilution with pristine matter; the positions in the Mg–Al plane supports this interpretation. For the three stars left, indicated with asterisks surrounded by circles, the interpretation of their position in the O–Al and Mg–Al planes leads to different conclusions. Looking at the O–Al plane, the comparison of data with the AGB chemistry suggests that the Al abundances are slightly overestimated (still within the error bars) and that they formed from an $\sim$50 per cent mixing of AGB ejecta and pristine matter. On the other hand, their surface magnesium reflects the chemistry of the AGB gas, with practically no dilution; in this case we should invoke an overestimation of their oxygen to allow consistency with the models. Our favourite option is the former, which is compatible with the large error bars of magnesium, relative to the overall Mg spread observed. This understanding is in

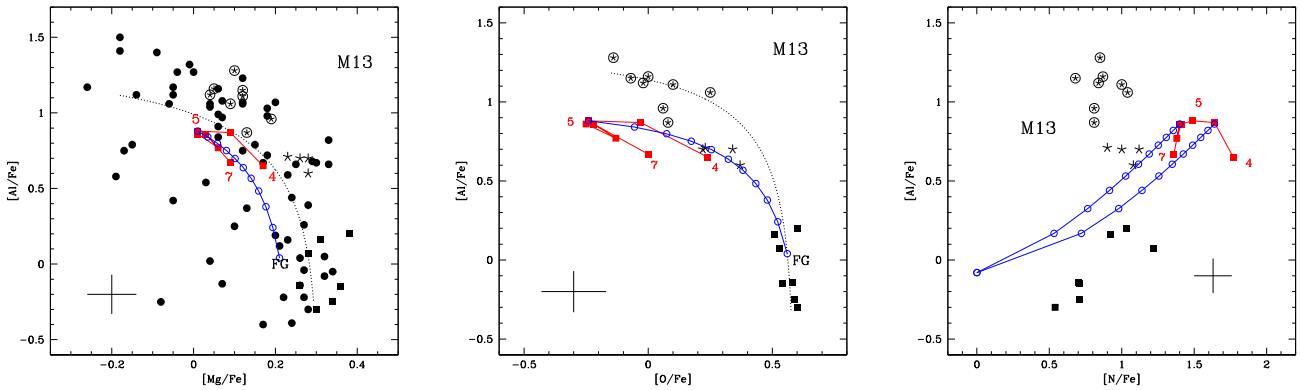

Figure 5. The Mg–Al (left), O–Al (centre), and N–Al (right) distribution of stars in M13. The observations are compared with AGB models of metallicity $Z = 10^{-3}$. The meaning of the symbols is the same as in Fig. 4.

agreement with the studies by Boberg, Friel & Vesperini (2016), who suggest that SG stars in M53 formed from gas diluted with pristine matter, and by Caloi & D'Antona (2011), that, based on the analysis of the HB, concluded that only a small helium spread, $\delta Y \sim 0.04$, is present, thus ruling out the existence of a purely AGB contaminated stellar component. Concerning the bottom-right panel of Fig. 4, from the AGB ejecta, we expect a clear N–Al correlation, shown by SG stars of this cluster.

3.3 The intermediate metallicity GCS

We discuss M13, M2, and M3 together, owing to their close metallicities and chemical compositions. The pattern traced by the multiple populations of the GCs considered in this section will be discussed on the basis of their intermediate metallicity, i.e. $Z = 10^{-3}$. These models were calculated ad hoc for the distribution of Mg, Al, and O shown in these clusters (see Table 1), slightly enhanced in Mg with respect to those used in Ventura et al. (2016). As shown in Fig. 1, the HBB temperatures of stars of this metallicity are not sufficient to allow any silicon production, if not in the stars of mass close to the threshold for core collapse. This is confirmed by the results for these three clusters, indicating that no silicon spread is observed. Therefore, we will focus our analysis on the Mg–Al plane and on the abundances of the elements involved in CNO cycling.

3.3.1 M13

The M13 sample is composed of 81 stars, for which the Mg and Al abundances were calculated. For 18 of these sources the CNO abundances are also available. The distribution of the data points on the Mg–Al, O–Al, and N–Al planes is shown in Fig. 5; overimposed to the data, we show the yields from massive AGBs.

In the Mg–Al plane (see the left-hand panel of Fig. 5) we report the results of the fit, with $[\mathrm{Al/Fe}]_{\mathrm{SG}} = 1.29 \pm 0.04$ with rms=0.56. Form this panel we note that the yields from AGB stars show up a depletion of magnesium of ~ -0.2 dex, which is sufficient to reproduce the majority of the stars in the sample, with the exception of $\sim$10 stars, in which the measured Mg is $\sim$0.4 dex smaller than the average of FG stars, as given by ME15. These stars are located in the left, upper zone of the Mg–Al plane, with [Mg/Fe] < 0; their Al abundances are $\sim +0.3$ dex larger than the Al content of the yields. The data errors seem not sufficiently large to explain this difference.

In the O–Al plane[9] we see that the observed O spread, δ[O/Fe] ~ -0.7 dex, is well reproduced by the AGB models. This comparison suggests the presence of SG stars in M13, some of which were likely formed from the AGB ejecta, with a small (if any) degree of dilution with pristine gas. However, this result must be taken with some caution. The smallest Mg abundances measured for the 10 stars mentioned above would indicate that the AGB nucleosynthesis at the intermediate metallicities, while correctly predicting the depletion of oxygen, slightly underestimates the strength of Mg burning. We expect that these stars have δ[O/Fe] > -0.8; unfortunately for none of the $\sim$10 Mg-poor stars discussed above the CNO data is available to draw firm conclusions in this regard.

As shown for M53, a correlation pattern is expected from the AGB ejecta in the N–Al plane, as displayed in the right-hand panel of Fig. 5. This is also confirmed by previous studies on these two elements (e.g. Bragaglia et al. 2010; Gratton et al. 2012). Nevertheless, no clear distinction between FG and SG stars is detected in the distribution of the N abundances of this cluster. This suggests that the N abundances should be revisited and avoid us to draw any firm conclusion in this regard.

M13 has traditionally played an important role in the studies focused on GCs, particularly for the complex morphology of the HB, which displays an extended blue tail. On the side of the chemical patterns traced by GC stars, early results presented by Kraft et al. (1997) showed an extended O–Na anticorrelation, with an oxygen spread of δ[O/Fe] ~ -0.8 dex, very similar to that shown in Fig. 5 (see the middle panel); a less defined, albeit statistically significant Mg–Al trend is found in the same work, with an overall Mg and Al spreads δ[Mg/Fe] ~ -0.4 dex and δ([Al/Fe]) $\sim +1.2$ dex, again in agreement with the results from ME15. Important results from high-resolution spectroscopy of M13 giant stars were published by Sneden et al. (2004) and Cohen & Meléndez (2005b) that confirmed the existence of an O–Na anticorrelation pattern, with the same oxygen and Na spreads given in Kraft et al. (1997). In both studies the stars with the largest sodium are magnesium poor, with the same Mg spread, δ[Mg/Fe] ~ -0.4 dex, found by ME15. A slightly lower Mg spread was detected by Johnson et al. (2005).

In all the aforementioned investigations, the largest abundances of magnesium are [Mg/Fe] $\sim +0.4$, higher than the Mg of FG stars given by ME15, on which we based our computations; while this

[9] $[\mathrm{Al/Fe}]_{\mathrm{SG}} = 1.18 \pm 0.03$ with rms=0.28.

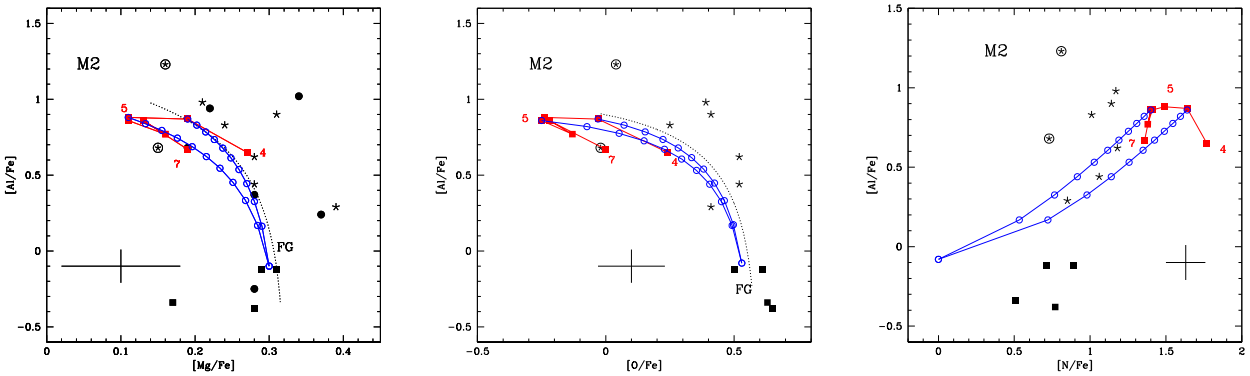

Figure 6. The Mg–Al (left), O–Al (centre), and N–Al (right) distribution of stars in M2. The observations are compared with AGB models of metallicity $Z = 10^{-3}$. The meaning of the symbols is the same as in Fig. 4.

difference has practically no effects on the Mg spread, Al production is affected by this choice, because a higher Al is expected when the initial Mg is larger. This could reconcile the largest Al given in ME15 with the AGB yields.

These studies, although less homogeneous and with a lower statistics than ME15, confirm the oxygen and magnesium spreads given in ME15. As stated previously, while the oxygen spread is nicely reproduced by the AGB models of the M13 metallicity, the expected Mg spread is too small to reproduce the stars with the most extreme chemical composition; this is indeed not new, as the same problem was addressed by Ventura, Carini & D'Antona (2011), when comparing the AGB ejecta with the most Mg-poor stars in M13 and NGC2808. The analysis by Ventura et al. (2011) showed that the key quantity relevant for the determination of the overall Mg depletion in the gas from massive AGB stars is the cross-section of the ^{25}Mg(p, γ)^{26}Al reaction; this is because a significant depletion of the total magnesium is made possible only via an efficient destruction of the ^{25}Mg produced by ^{24}Mg burning. An analysis of the enhancement of the ^{25}Mg destruction rate required to reproduce the observed Mg spread is in progress (Ventura et al., submitted for publication).

Taken as a whole, the results by ME15, in agreement with the previous works cited above, indicate that M13 harbours a significant fraction of SG stars; this is in agreement with the recent analysis by Milone et al. (2017), who suggest that only ∼20 per cent of the stars in M13 belong to the FG of the cluster. The wide oxygen and magnesium spreads observed indicate that part of SG stars formed from almost pure AGB ejecta, thus suggesting the presence of an extremely rich population. This is in agreement with the study by Caloi & D'Antona (2005), who claimed the presence of stars significantly enriched in helium to account for the complex morphology of the HB of M13. A later analysis by Dalessandro et al. (2013), aimed at interpreting UV, HST data, confirmed the presence of stars enriched in helium, although the largest helium proposed, $Y_{\rm max} = 0.30$, is slightly smaller than the helium expected in stars formed from pure AGB ejecta. Our interpretation is much more consistent with the study by D'Antona & Caloi (2008) that suggest the presence of a fraction of M13 stars with helium mass fractions in the range $0.27 < Y < 0.35$.

3.3.2 M2

Data for M2 are limited to 18 stars, 12 of which have the CNO abundances. This will allow us to undergo a less robust and complete analysis, compared to M13 and M3.

The comparison with the chemical composition of the AGB ejecta is shown in Fig. 6. To account for the slightly higher magnesium of FG stars in M2 compared to the other intermediate metallicity clusters, we shifted all the AGB magnesium by +0.1 dex; we warn here that while this choice does not alter the results regarding the Mg depletion, it is going to underestimate the Al content of the ejecta, which is practically independent of the initial aluminium whereas it is extremely sensitive to the magnesium initially present in the star.

The data in the Mg–Al and O–Al planes[10] trace two well-defined anticorrelation patterns. Five stars (indicated with full squares in Fig. 6) belong to the FG, while the 13 left (asterisks) show evidences of proton-capture processing. The chemical composition of the two stars with the most extreme chemistry (2M21332216-0048247 and 2M21332527-0049386), with δ[Mg/Fe] = −0.15 and δ[O/Fe] = −0.5, is compatible with dilution of gas from AGB with ∼30 per cent of pristine matter; these stars are indicated with asterisks+circles. The paucity of data in this case prevents any conclusion regarding a possible discreteness in the distributions of the data on the planes.

In the N–Al plane, while FG and asterisk stars show [N/Fe] values more compatible with the correlation pattern traced by the dilution curves, this is not true for two O-poor stars in particular (2M21332216-0048247 and 2M21332527-0049386). This should indicate possible problems in the determination of N abundances for the most extreme chemistry stars.

Lardo et al. (2013) claimed evidences of multiple populations in M2, based on the splitting of the RGB and a well-defined C–N anticorrelation. High-resolution spectroscopy of M2 stars was presented by Yong et al. (2014), who outlined the presence of the classic O–Na anticorrelation and of a Na–Al correlation trend; the Mg–Al trend was not clear. In the same study, Yong et al. (2014) identified a stellar component enriched in iron (δ[Fe/H] ∼ +0.7 respect to the main peak, [Fe/H] = −1.7), whose numerical consistency is however below 5 per cent; because of such a small percentage, and taking into account that all the M2 stars in the ME15 sample share the same iron content ([Fe/H] ∼ −1.5 ± 0.15), we may safely neglect it in the present analysis. Pancino et al. (2017) have recently confirmed the presence of a clear Mg–Al anticorrelation in this cluster, analysing the data from *Gaia*-ESO survey. This is extremely important for our analysis, because in this metallicity

[10] [Al/Fe]$_{\rm SG}$ = 1.15 ± 0.11 with rms=0.5 and [Al/Fe]$_{\rm SG}$ = 0.9 ± 0.07 with rms=0.35, in the Mg–Al and O–Al planes, respectively.

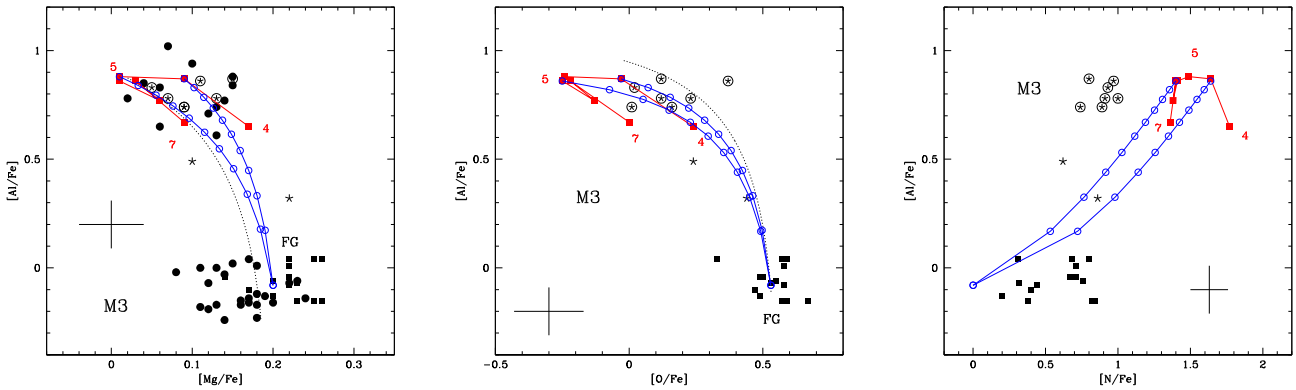

Figure 7. The Mg–Al (left), O–Al (centre), and N–Al (right) distribution of stars in M3. The observations are compared with AGB models of metallicity $Z = 10^{-3}$. The meaning of the symbols is the same as in Fig. 4.

range the Mg–Al trend is a valuable indicator of the nucleosynthesis experienced by the material from which SG stars formed. The Mg–Al anticorrelation traced by M2 stars is nicely reproduced by the AGB gas of the proper metallicity; the same holds for the O–Al pattern. The extent of the Mg and O depletion requires mixing of the AGB ejecta with $\sim 20 - 30$ per cent of pristine gas: this mixing would produce SG stars with a helium spread up to $Y \sim 0.32$, which is in excellent agreement with the results found by Milone et al. (2015) for this cluster.

3.3.3 M3

ME15 measured the abundances of a large number of stars (59) in M3. The data for M3 stars and the comparison with the AGB models are shown in Fig. 7.

The left-hand panel of Fig. 7 shows a clear Mg–Al anticorrelation,[11] with a maximum magnesium spread δ[Mg/Fe] ~ -0.2 and an overall Al increase of δ[Al/Fe] ~ 1. This is an indication that the gas from which SG stars formed was exposed to nuclear activity, with a less advanced nucleosynthesis compared to the clusters analysed previously, that exhibited traces of a much stronger Mg depletion. The stars with the most extreme chemistry are reproduced by mixing AGB gas with a small percentage (below 20 per cent) of pristine matter. The distribution of the stars in the Mg–Al plane suggests a gap in the star formation history, which prevented star formation from dilution with a large fraction of pristine gas; confirmation of this result requires more statistics, possibly accompanied with a detailed analysis of the distribution of the stars in the CMD.

The ME15 data in the O–Al plane,[12] shown in the middle panel of Fig. 7, trace a clear anticorrelated pattern. The AGB models can nicely reproduce the maximum oxygen spread observed, δ[O/Fe] ~ -0.4 dex: in this case a higher fraction of pristine gas is required to reproduce the O abundances of the stars with the highest Al, compared to what we found in the Mg–Al plane. Even in this case we note the clear distinction between the FG and the group of stars with [Al/Fe] $> +0.7$. Only two stars, marked with an asterisk, show an intermediate chemistry in the Mg–Al and O–Al planes, in agreement with a higher degree of dilution with the pristine gas. In the right-hand panel of Fig. 7, N–Al correlation is displayed by the data. FG stars show the lowest [N/Fe] values (in a range compatible with the effect of deep-mixing), while the Al-rich group of stars shows a somewhat lower N respect to the expectation.

The presence of stars with a small content of Mg and O and with large abundances of Al is a clue of the presence of an SG in M3. The Mg–Al anticorrelation in M3 is clearly bimodal, as M4 (e.g. Villanova & Geisler 2011), at odds with all the others GCs presented in this work. The data by ME15 confirm star-to-star differences, as in the study by Cohen & Meléndez (2005b), who found an O–Mg correlation and an O–Na anticorrelation in the chemical composition of giant stars in M3. Indications of the presence of stars formed from processed gas were also found by Johnson et al. (2005), who claimed the detection of a Mg–Al anticorrelation, although the scatter in magnesium was not fully confirmed. On the photometric side, a recent study by Massari et al. (2016) outlined the presence of at least two stellar populations in M3.

While the presence of SG stars in M3 is definitively confirmed by the investigations mentioned above and the ME15 data, the modality with which the SG formed is far from being clear. The analysis of the Mg–Al plane suggests that SG stars formed from basically pure AGB gas, whereas from the O–Al data we deduce that significant dilution is required. We are much more favourable to the second possibility, because the formation of stars from undiluted AGB ejecta would imply the presence of a helium-rich population, which is ruled out by the morphology of the HB of this cluster, which was shown to be well reproduced by the use of a small helium dispersion. An $\sim$50 per cent dilution with pristine gas would imply a maximum helium $Y \sim 0.30$, the same quantity invoked by Caloi & D'Antona (2008) to explain the bluest stars in the HB of M3. The presence of stars with this helium enrichment is at odds with the conclusions by VandenBerg et al. (2016); Valcarce et al. (2016); Denissenkov et al. (2017), who claim a very small dispersion $\delta Y < 0.02$ to explain the distribution of the stars along the HB.

3.4 M5: another cluster on the edge?

The large number of stars observed (122) for M5 allows a solid interpretation of the different populations present in this cluster. The results of the comparison of the distribution of the data points with the chemistry of AGB stars of the same metallicity ($Z = 1.5 \times 10^{-3}$) are shown in the three panels of Fig. 8.

The most relevant difference in the comparison with the clusters analysed so far is that only a small Mg depletion is observed: ME15 claim that the magnesium difference between FG and SG stars is

[11] [Al/Fe]$_{SG} = 0.87 \pm 0.03$ with rms=0.4.
[12] [Al/Fe]$_{SG} = 0.95 \pm 0.04$ with rms=0.34.

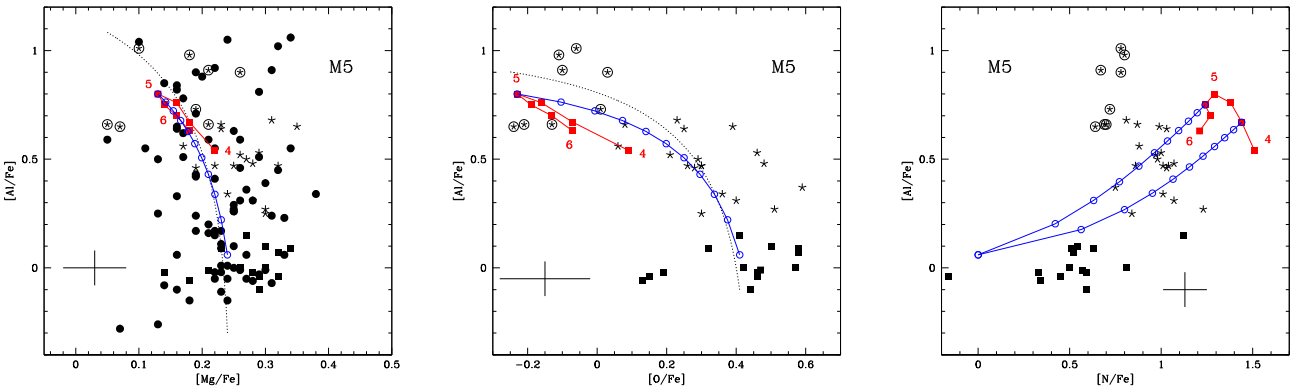

Figure 8. The Mg–Al (left), O–Al (centre), and N–Al (right) distribution of stars in M5. The observations are compared with AGB models of metallicity $Z = 1.5 \times 10^{-3}$. The meaning of the symbols is the same as in Fig. 4.

below 0.1 dex for M5. Conversely, the Al spread is large, with a few stars having [Al/Fe] ~ 1.[13] This is what we would expect if the gas from which SG stars formed was expelled by AGB stars. Within massive AGB stars with the metallicity of M5 ([Fe/H] $= -1.25$) we find that Mg burning and Al production are activated, but the temperatures are not sufficiently hot to allow a very advanced nucleosynthesis, with a strong reduction of the surface magnesium. This is the reason why the distribution of the stars in the Mg–Al is almost vertical. Note that the small depletion of magnesium is not at odds with the large spread in aluminium: as discussed previously, the initial Mg is much higher than Al, thus the consumption of an even small amount of Mg is enough to produce large quantities of Al.

The small spread in magnesium makes the O–Al plane[14] the most suitable to infer the presence of multiple population in M5 and, more generally, in higher metallicity GCs. In this regard, the results from AGB modelling allow a nice fit of the distribution of stars in the O–Al plane, particularly in the interpretation of the stars with largest Al, thus with the most extreme chemical composition, which shows a reduction of oxygen δ[O/Fe] ~ -0.6 dex. We see in the central panel of Fig. 8 that the dilution curve well reproduce the O–Al pattern traced by the observations. The almost uniform spread of the data across the dilution curve suggests a continuous process of formation of the SG, with different degrees of dilution of gas from AGB stars and pristine gas, in agreement with the preliminary findings by Ventura et al. (2016).

Taking together, the O–Mg–Al data indicate that M5 stars have a peculiar metallicity: massive AGB stars sharing this chemical composition experience HBB sufficiently strong to consume oxygen and to produce aluminium, but the HBB temperatures do not allow a significant depletion of magnesium.

Similarly to the previous cases (M13 and M2), even in this cluster the N measurements by ME15 of the Al-rich/O-poor group of stars are once more against our immediate understanding. They are less enriched in nitrogen than the remaining SG stars; we believe that more reliable N measurements are needed to draw any conclusion in this regard.

The above results, particularly the presence of stars with an oxygen content 4 times smaller than FG stars and aluminium mass fractions 10 times larger, indicate that M5 harbours SG stars. This is not surprising, as high-resolution spectroscopy outlined an O–Na anticorrelation among RGB stars (Carretta et al. 2009a) and HB stars (Gratton et al. 2013); interestingly, the latter study shows that the stars with the anomalous chemical composition populate the blue side of the HB, as expected based on their higher helium.

The presence of stars with a variety of O abundances (see the middle panel of Fig. 8), when compared with the chemistry of the AGB ejecta, leads us to the conclusion that the SG in M5 formed with various degrees of dilution of AGB gas with pristine matter, and that some stars with almost a pure AGB chemical composition formed. If part of the SG formed from the AGB ejecta without dilution, the duration of the process must have been longer than $\sim 30 - 40$ Myr: a shorter process, as discussed in Section 2.3, would imply the presence of a group of stars extremely enriched in helium, which is ruled out based on the studies focused on the morphology of the HB of M5, indicating that the largest helium of SG stars in this cluster is $Y \sim 0.31$ (D'Antona & Caloi 2008). This is consistent with the helium in the ejecta of lower mass AGB stars, which evolve on time-scales of the order of $\sim 30 - 40$ Myr.

Concerning the helium content of M5 stars, we find that the spread invoked by Lee (2017) to explain the morphology of the RGB bump is too small ($\delta Y \sim 0.04$) to allow compatibility with the presence of stars with very low oxygen abundances.

3.5 M107: magnesium off the game

This cluster is one of the two with the highest metallicity ([Fe/H] $= -1$, corresponding to $Z = 2.5 \times 10^{-3}$) in the ME15 sample. The entire sample is made up of 42 stars; for 12 of them the measurements of CNO are available. We prefer to concentrate on the latter, smaller subsample for the analysis of this cluster, because ME15 found a trend of the Mg abundances with the effective temperature, which required some ad hoc corrections. We compare the data with the massive AGB yields of the proper metallicity in the three panels of Fig. 9.

No Mg–Al anticorrelation is found among the observed values (see the left-hand panel of Fig. 9), in agreement with AGB models, according to which at these metallicities the HBB temperatures are too cool to allow any significant depletion of magnesium (see Fig. 1).

The Al-spread, if present, is very small: this is the first case within the present work, where it is difficult to distinguish the different populations in the Mg–Al plane. Note that the AGB yields, run with the Al of the stars in the FG of the cluster, are enriched in aluminium with respect to the FG, with δ[Al/Fe] $\sim +0.4$ dex; this is shown in the left-hand panel of Fig. 9.

[13] [Al/Fe]$_{SG} = 1.08 \pm 0.04$ with rms=0.5.
[14] [Al/Fe]$_{SG} = 0.9 \pm 0.03$ with rms=0.38.

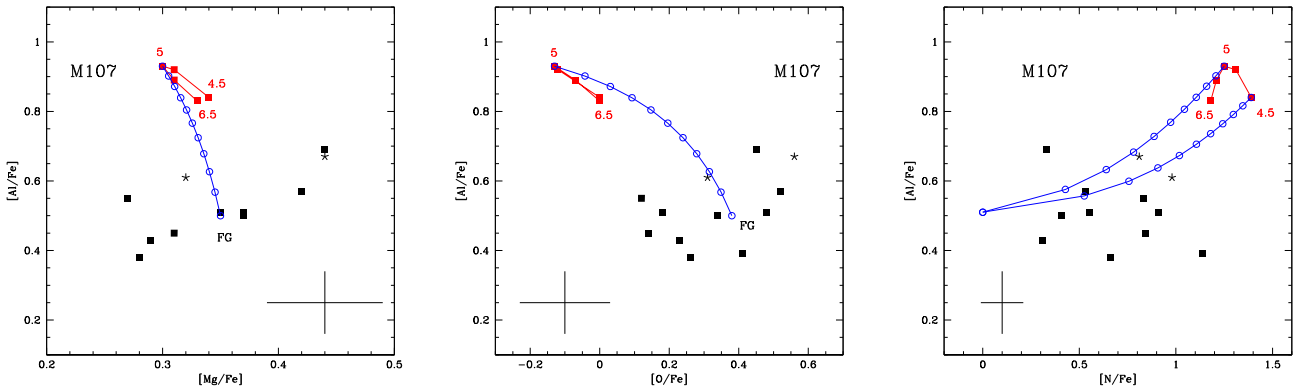

Figure 9. The Mg–Al (left), O–Al (centre), and N–Al (right) distribution of stars in M107. The observations are compared with AGB models of metallicity $Z = 2.5 \times 10^{-3}$. The meaning of the symbols is the same as in Fig. 4.

For the metallicity of M107 stars, based on the arguments given in the previous section, we find that the depletion of oxygen is a much more valuable indicator of the degree of contamination of SG stars, compared to the Mg spread: as shown in the middle panel of Fig. 9, the AGB yields are expected to show the imprinting of O-depletion, with δ[O/Fe] ~ -0.5 dex and, more generally, a O–Al trend, which is indeed not observed. On the contrary, the data points cluster around the chemistry of the FG of the cluster, a strong hint that either M107 is a FG-only cluster or it hosts SG stars formed with a large degree of dilution of AGB gas with pristine matter.

Note that the present conclusions are different from what deduced by Ventura et al. (2016) that SG stars definitively exist in M107: that result was based on the assumption that no Al-enhancement would be expected in metal-rich clusters if the initial Al is higher than solar-scaled, whereas the present results, self-consistently based on AGB models with the same initial Al of FG stars, partially disregard that assumption.

The data shown in the N–Al plane (see the right-hand panel of Fig. 9) seems to confirm the conclusion drawn based on the distribution of the stars in the O–Al plane. Any SG star should be enriched in both N and Al, according to the dilution curve shown in the figure. On the contrary, we note that the data points do not show any significant spread in Al, whereas the N-enrichment ranges from δ[N/Fe] $\sim +0.3$ to δ[N/Fe] $\sim +1$: the only possible explanation is that either the N-rich star are FG stars, which were subject to deep mixing during the RGB phase, or they belong to the SG of the cluster, formed from AGB gas largely diluted with pristine matter. The latter explanation likely holds for the two stars showing an Al-excess, indicated with asterisks in the figure.

In the case of M107, no deep analysis of the HB is present in the literature, thus the conclusions given above cannot be tested against any result from photometry. While the lack of any Mg and probably Al spread is in agreement with the expectations if AGB stars were the polluters, the lack of SG stars with the chemical composition of pure AGB ejecta prevents a solid evaluation of the reliability of the AGB stars of this metallicity.

3.6 M71

The metallicity measured for M71 is [Fe/H] ~ -0.7. This is the highest metallicity cluster in the sample we have considered. Theoretically, this represents a very useful case, to understand how self-enrichment works in high metallicity GCs, and to confirm further how the chemistry of self-enrichment changes with the metallicity of the cluster. Unfortunately only for seven stars we have the determination of all the chemical abundances, including the CNO elements. This partly prevents a solid understanding of how the SG formed in this cluster.

The data available show no sign of Mg-dispersion, in agreement with Carretta et al. (2009b) and with the expectations: this cluster is even more metal-rich than M107, which also shows no Mg dispersion.

We show the data points of M71 stars in Fig. 10; the yields from AGB stars of the same metallicity ($Z = 6 \times 10^{-3}$) are also shown. The analysis of a possible pollution from AGB stars is not straightforward in this case, because the expected Al enhancement (δ[Al/Fe] $\sim +0.2$) and oxygen depletion (δ[O/Fe] ~ -0.3 dex) are only slightly higher than the errors associated with the data for the two elements.

The simultaneous analysis of the O–Al and N–Al planes allows us to better identify stars that show the imprinting of AGB pollution with a partial dilution with the pristine gas. This is the case of the stars marked with the asterisk. In the O–Al plane we clearly identify 3 FG stars, indicated with solid squares. The four stars left, indicated with asterisks, show up an anomalous chemical composition, which might suggest that they belong to the SG of the cluster. One of the stars (2M19535064+1849075) shows an enhancement in aluminium and a depletion of oxygen compatible with AGB gas 50 per cent diluted with pristine matter. For the two stars with slightly enriched in aluminium (2M19535764+1847570 and 2M19533986+1843530), the possibility that they belong to the FG holds only if their oxygen is overestimated: alternatively, they are FG stars, with the Al content overestimated by ∼0.1 dex. While the error bars are sufficiently large to make both cases possible, we are more confident about the first possibility, because of the simultaneous Al and N enrichment of these stars (see the right-hand panel of Fig. 10).

In the N–Al plane these three stars show both the enhancement in nitrogen ([N/Fe] $\sim$ 1.1) and aluminium ([Al/Fe] $\sim$ 0.5), which correspond to ∼50 per cent of pollution from AGB stars. One of the three stars discussed (2M19535064+1849075) is also depleted in oxygen ([O/Fe] $\sim$ 0.45) in nice agreement with the dilution curve, while the other two stars show initial abundances of oxygen ([O/Fe] $\sim$ 0.6) likely overestimated (this is not an issue though, if we take into account the error bars). On the contrary, one star (2M19534827+1848021) shows the evidence of oxygen depletion and nitrogen enhancement, while aluminium appears to be almost not touched ([Al/Fe] $\sim$ 0.35).

The possibility that SG stars in M71 formed from the AGB ejecta was first invoked by Boesgaard et al. (2005) to explain the

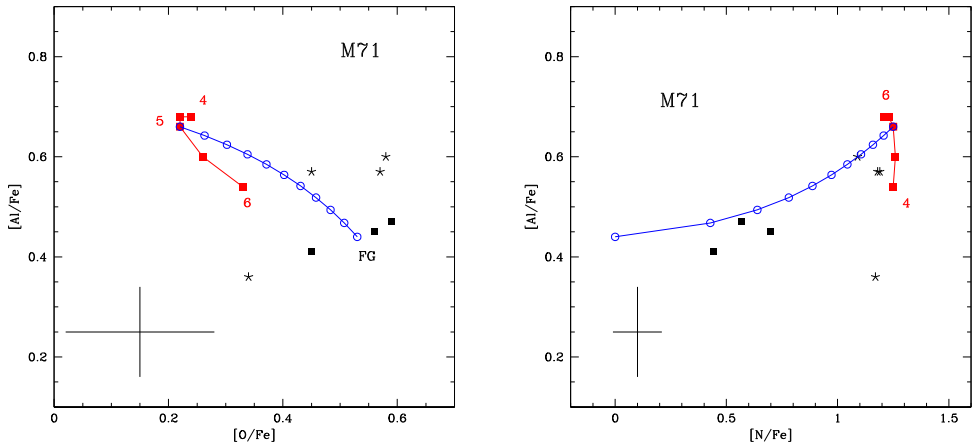

Figure 10. The O–Al (left) and C–N (right) distribution of stars in M71. The observations are compared with AGB models of metallicity $Z = 6 \times 10^{-3}$. The meaning of the symbols is the same as in Fig. 4.

abundances of αelements and neutron capture elements. In a more recent study, Alves-Brito et al. (2008) detected CN–Na and Al–Na correlations among RGB stars below the bump, a clue of the presence of SG stars. The present data, within the context of the self-enrichment by AGB stars, confirm the presence of SG stars and indicate that some dilution is required to model the most extreme chemical compositions. On the other hand, the robustness of this conclusion is partly affected by the small O and Al spread expected in metal-rich environments, which are unfortunately comparable with the extent of the error bars. The observation of a much higher number of stars is required to make this conclusion more reliable on the quantitative side.

4 THE 'CLASSIC O–NA ANTICORRELATION IN GC STARS

Before entering the discussion of the implications of the results presented so far, we want to further test the hypothesis that pollution from massive AGB stars provided the contaminating material from which SG stars formed in GCs, by comparing the yields of these stars with the O–Na pattern traced by GC stars.

Unfortunately, the ME15 APOGEE abundances data set do not include the Na measurements because the Na spectral lines present in the *H*-band are too weak (even for the most metal-rich GCs like M107 and M71; see ME15 for more details). Thus, we are forced to consider complementary optical data (see below) that are not fully homogeneous with those used so far. On the other hand, while the main conclusions will be drawn based on APOGEE data solely, we believe important to present this further test, because the O–Na anticorrelation has traditionally being considered as the key signature of the GCs chemical patterns, as it has been observed in practically all GCs so far studied in the literature (e.g. Carretta 2006; Gratton et al. 2012).

Understanding the behaviour of Na in massive AGB stars is not trivial, because the surface abundance of this species stems from the equilibrium between the production and the destruction channels. The former is mainly determined by ^{22}Ne proton capture activity, whereas the latter is made up of two proton capture reactions by Na nuclei, the dominant channel being the Na$(p, \alpha)^{20}$Ne reaction (Hale et al. 2002, 2004).

The synthesis of Na is favoured until temperatures $T \sim$ 100–110 MK, whereas the destruction prevails in hotter environments. In low-metallicity massive AGB stars, Na increases during the initial AGB evolution, owing to ^{22}Ne burning, then decreases in the later phases, when the destruction channel becomes dominating (Ventura & D'Antona 2006).

What renders tricky the interpretation of the results is that there is no clear trend of the behaviour of Na with mass and metallicity: while AGB yields generally produce Na-rich gas, the production factor with respect to the Na initially present in the star depends on the duration of the phase during which the temperature of the base of the envelope exceeded the threshold given above: the longer was this phase, the smaller will be the average Na in the gas lost.

If we consider the clusters on which this study is based, the compilations by Carretta et al. (2009a,b) include data for M15, M5, M107, and M71. Fig. 11 shows the data from Carretta et al. (2009a,b),[15] overimposed to the yields of AGB stars of the appropriate metallicity for each cluster. An offset among the [O/Fe] abundances is found between the two samples (APOGEE versus Carretta et al.). Because of the different methods used in the chemical analysis (e.g. EWs versus spectral synthesis, estimation of the stellar parameters, model atmospheres, spectral range, solar reference abundances, etc.), this is somewhat expected. Besides that, the APOGEE O abundance is obtained from the near-infrared OH molecular lines that are likely more affected by 3D/NLTE effects than the optical [OI] 630 nm line; see e.g. Dobrovolskas et al. (2015), who found that O-abundances from OH lines could be ∼0.2–0.3 larger than the optical [OI] line in metal-poor ([Fe/H] <-2.5) stars. This should be kept in mind when comparing [O/Fe] from optical works, as Carretta et al. (2009a,b), with APOGEE.

We start from M107 and M71, the two highest metallicity clusters in this group. The chemistry of the yields of stars of different mass is pretty similar in these cases (Ventura et al. 2013), because the metallicity is sufficiently large that the destruction channel of Na is never fully activated during the AGB phase, not even in the most massive stars. This makes the comparison between the data and the yields very simple, as also the trend of the dilution curve, giving the results expected when the gas from AGB stars is mixed with pristine matter in the cluster.

For both M107 and M71 we find that the trends defined by the data from Carretta et al. (2009a,b) on the O–Na plane are nicely

[15] For stars in common between Carretta et al. (2009a) and Carretta et al. (2009b), we show the results from the latter where the [O/Fe] and [Na/Fe] are obtained with a higher level of accuracy.

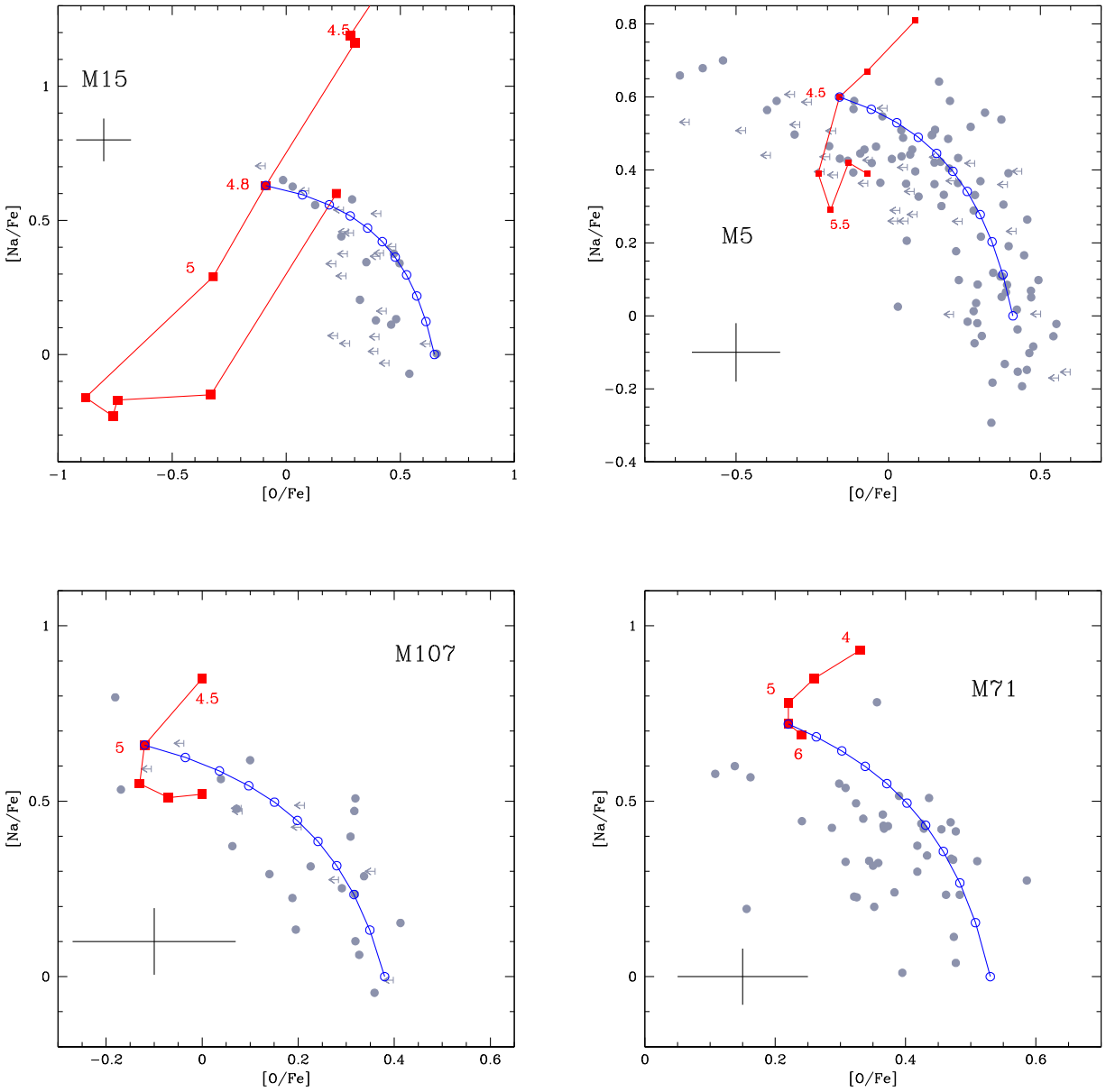

Figure 11. Data set from Carretta et al. (2009a,b) in the O–Na plane are shown in grey for M15 (top-left), M5 (top-right), M107 (bottom-left), and M71 (bottom-right). Upper limits in O abundances are shown as arrows; detections are indicated as circles. AGB yields (red squares) and their corresponding dilution curves (blue open circles) are also shown according to the metallicity of each cluster.

reproduced by the yields of AGB stars. In particular, the latter can account for the observed spreads in oxygen (δ[O/Fe] ~ -0.55 and δ[O/Fe] ~ -0.35, respectively, for M107 and M71) and Na (δ[Na/Fe] $\sim +0.7$ in both clusters).

Fig. 11 (as compared to the findings based on APOGEE data only) allows a deeper analysis of the possible presence of multiple populations in these clusters. In Sections 3.5 (M107) and 3.6 (M71), we found that the few stars observed by APOGEE belong to the FG, while from the O–Na data (with much better statistics; see Fig. 11) we can conclude that both clusters harbour a significant fraction of SG stars; part of which (those with the lowest O and highest Na) formed from gas with a small degree of dilution with pristine matter.

Turning to M5, the O–Na data, shown in the top, right-hand panel of Fig. 11, trace a well-defined anticorrelation pattern, the spreads in oxygen and Na being, respectively, δ[O/Fe] ~ -1 and δ[Na/Fe] $\sim +0.6$. The dilution pattern between the yields of AGB models of the same metallicity as M5 stars and pristine matter can account for most of the observed stars, with the exception of a few objects exhibiting an oxygen depletion of a factor of $\sim$10 with respect to the FG, a factor of 2 in excess of the theoretical expectations. We propose that the stars with the unusually low oxygen content are SG stars of the cluster, which underwent deep mixing during the RGB ascending, owing to the lower entropy barrier left behind by the first dredge-up, as a consequence of the higher initial helium. As shown by D'Antona & Ventura (2007), such a deep mixing in SG stars would provoke a significant decrease in the surface oxygen, leaving the Na content practically unchanged.

The explanation of the distribution of stars in the O–Na plane is consistent with the discussion on the APOGEE data of M5 stars, addressed in Section 3.4, that this cluster harbours SG stars formed

with a variety of dilution factors of AGB gas with pristine gas, including also stars with a chemical composition very similar to the AGB ejecta.

The interpretation of the O–Na observations of M15 stars is more cumbersome, because the Na yields at these low metallicities are extremely sensitive to the mass of the star (see the bottom, left-hand panel of Fig. 11). This is related to the above-discussed competition between the production and destruction channels of Na, because the higher mass AGB stars of this metallicity reach at the base of the envelope temperatures sufficiently large (see Fig. 1) that the destruction channel prevails for a significant part of the AGB evolution, thus producing Na-poor ejecta. The trend of the Na yields with mass is further complicated by the strong winds suffered by the most massive AGB stars, which favour the loss of the external mantle before a significant destruction of the Na accumulated in the surface regions during the early AGB evolution may occur.

As shown in Fig. 11, the Na yields span an interval in excess of 1 dex, ranging from $\sim 6M_{\odot}$ stars, for which δ[Na/Fe] ~ -0.2, to $\sim 4.5M_{\odot}$ stars, for which δ[Na/Fe] $\sim +1$. The interpretation of the observations in the context of the self-enrichment by AGB stars in this case would require the details of the timing of the formation of SG stars, i.e. when the formation of SG started and when the gas from AGB began to mix with pristine matter. This effort is clearly beyond the scope and the possibilities of the present analysis.

5 DISCUSSION

The sample by ME15 offers a valuable opportunity to understand the formation of multiple population in GCs, given the wide range of metallicities, covering the interval $-2.4 <$ [Fe/H] < -0.7. The simultaneous knowledge of the abundances of various chemical elements allows a full, though more complex analysis, not limited to the interpretation of a single observational plane.

Moving across the different clusters, we find that the relative importance of the data on a given chemical species depends on the metallicity. The silicon spread is a key indicator of what was going on during the formation of metal poor GCs, the Mg–Al trend was crucial to reconstruct the star formation history in intermediate-metallicity clusters, whereas the analysis of more metal-rich GCs relies essentially on the extent of the O–Al anticorrelation.

Nitrogen deserves a separate discussion. During the RGB ascending the surface N of stars undergoes significant variations, owing to convective mixing of the envelope with stellar regions exposed to nuclear activity. This prevents a straightforward use of the N data to deduce the initial chemical composition of the star. However, the ejecta of metal-poor AGB stars are expected to be largely enriched in nitrogen, up to a factor $\sim$100 or more, compared to the initial abundance. Giants formed with so large quantities of nitrogen are not expected to undergo any change in the surface N, because any deep mixing would reach internal, CNO processed material, where the equilibrium N is not overabundant with respect to the surface content. Therefore, reliable measurements of the surface N in low-metallicity ([Fe/H] < -1) GCs would definitively help in understanding whether star formation from polluted gas occurred, providing also indications on the degree of dilution with pristine matter.

In the present analysis we describe how the formation of the SG depends on the metallicity of the cluster, checking for compatibility among the data and the predictions of the self-enrichment scenario by massive AGB stars. The ME15 is particularly suitable to this aim, because among the various actors proposed so far to explain the formation of multiple populations in GCs, the ejecta of massive AGB stars, as discussed in Section 2.2, are those most sensitive to the chemical composition of the stars.

In the comparison between the expected and observed variations in the light elements abundances, we have to keep into account that the abundances of SG stars with the most extreme chemistry are determined by two factors: (a) the nature of the polluters, which reflects into the chemical composition of the ejecta; and (b) the degree of dilution of the gas ejected with pristine matter of the cluster, sharing the same chemical composition of FG stars.

The maximum spread of each element for the individual GCs would correspond to the quantities predicted by the AGB ejecta of the same metallicity only in case that SG stars with no dilution formed, which is expected to occur only in a limited number of cases. When dilution occurs, the chemistry of SG stars will be less extreme than the ejecta: what is relevant in confirming or disregarding any pollution scenario is that the spread for the various chemical elements in all the clusters is smaller than expected based on a pure contamination. This is indeed the case, with the only exception of the magnesium spread in M13 as discussed in Section 3.3.1.

The chemical composition of the ejecta from massive AGB stars presented here outlined a remarkable capability of following the trend with metallicity traced by data of stars in the GCs analysed by ME15.

(i) Strong HBB at the base of the envelope of metal-poor AGBs is capable of producing the silicon spread observed in the lowest metallicity clusters. As stated previously, given that silicon is one of the most abundant metals within the stars, an enhancement δ[Si/Fe] $\sim +0.2$ dex is the clue that the gas from which SG stars formed was exposed to a very advanced nucleosynthesis.

(ii) The temperatures at the bottom of the external mantle reached by AGB stars of metallicity [Fe/H] $= -2$ are sufficiently large to start an advanced Mg–Al nucleosynthesis, but not hot enough to produce any significant silicon enhancement. The analysis of the data shows a clear anticorrelation only in the lowest metallicity cluster.

(iii) In the intermediate metallicity GCs, we still see Mg–Al trend, but the magnesium spread is shorter than observed in more metal-poor GCs. This has a clear explanation from the results of AGB modelling, because a less advanced HBB nucleosynthesis is expected on higher metallicity AGB stars.

(iv) δ[Al/Fe] is observed to vanish in the highest metallicity clusters, suggesting a progressively lower Al self-enrichment process for the medium where SG form. This finds a confirmation in the AGB scenario: the strength of HBB becomes weaker and weaker as the metallicity increases, producing ejecta less rich in Al.

A more robust test of the self-enrichment by AGB stars demands more statistically significant data set of metal-rich clusters. The present sample includes only two metal-rich clusters, M107 and M71, with a small number of stars, and both characterized by a large dilution with pristine matter. The lack of any Mg and Si spread and a reduced O excursion in this kind of clusters would provide a more solid clue that AGB stars were the key polluters of intra-cluster medium of GCs, from which SG stars formed.

For all the clusters examined, we used the data of the stars with the most extreme chemical composition to infer whether direct formation of SG stars from the AGB ejecta occurred or, alternatively, which is the minimum dilution with pristine matter required. This is crucial to determine the largest helium enhancement expected for the most contaminated stars and offers a valuable opportunity to test the present conclusions with indirect estimates of the helium spread, based on the morphology of the HB. For the clusters for

which these estimates were available, it was possible to verify a satisfactory consistency.

The APOGEE data used in this work are of paramount importance, because they confirm that the material from which SG stars formed was exposed to a very advanced nucleosynthesis, with the activation of Mg burning and, in the most metal-poor clusters, the synthesis of silicon. This is of great help in the way towards the understanding of the possible GC polluters, because the possibility that either fast-rotating massive stars (Krause et al. 2013) or massive binaries (De Mink et al. 2009) played a role in this context can be ruled out. Indeed in neither of the two cases the temperatures of the nuclear burning regions are sufficiently hot to allow such an advanced nucleosynthesis.

The only possibility left besides the massive AGB scenario is super massive main sequence stars. As shown by Denissenkov & Hartwick (2014), the core temperature during H-burning reach ∼70 MK, thus triggering the activation of Mg burning and the production of aluminium. A straight comparison between the predictions of the AGB hypothesis and the chemical patterns expected when pollution from super massive stars is considered is cumbersome, because while it was shown that in the interiors of this class of objects the ignition of Mg burning occurs, the trend with metallicity, if any, needs further investigation. While in the AGB case the sensitivity of the HBB nucleosynthesis to the metallicity is a direct result of stellar evolution modelling, it is not clear how the chemical composition would affect the core H-burning of super massive stars. At the moment, this problem is still open.

6 CONCLUSIONS

We discuss the chemical composition of giant stars in nine Galactic GCs, for which the abundances of C, N, O, Mg, Al, and Si are available. The wide range of metallicities ($-2.4 < [Fe/H] < -0.7$) and the simultaneous knowledge of the elements mentioned above offer a valuable opportunity to test the origin of multiple populations in these complex stellar systems.

We concentrate on the possibility that the polluters of the intracluster medium, providing the gas from which SG stars formed, were massive AGB stars ($4\ M_{\odot} \leq M \leq 8\ M_{\odot}$), which experienced HBB at the base of their external envelope. To this aim, we calculated ad hoc AGB models, with the same metallicity and the same mixture of the stars belonging to the FG of each cluster.

In agreement with previous studies on GCs in the Milky Way, we find that all the clusters show the presence of SG stars, as deduced on the star-to-star chemical differences, which define abundance patterns in the different observational planes.

We find that the chemical patterns observed (Mg, Al, Si, and O in particular) are in good agreement with the theoretical expectations: (a) on the qualitative side, the spread observed for the different species follows the results from AGB evolution theories, according to which the strength of HBB, the phenomenon by which the contaminated gas is produced, becomes weaker the higher is the metallicity of the stars; (b) on a quantitative point of view, the spread observed for the various chemical species is in agreement with the chemistry of the AGB ejecta. The only exception to this is the Mg spread of M13 stars.

When available, we check consistency with results from photometry in the literature, particularly with the helium spread deduced on the basis of the morphology of the HB; this poses important constraints on the degree of dilution of the gas from AGB stars with pristine matter in the cluster, from which the SG formed.

A more solid confirmation of the general conclusions drawn in this work requires data for a larger sample of stars, particularly for metal-rich clusters: this is crucial to confirm that the extent of the spread observed between the chemical composition of FG and SG stars tends to vanish as the metallicity increases, as expected based on the results of AGB modelling. In addition, the lack of a clear N–Al correlation in the ME15 data, which has been previously confirmed in the literature and it is expected also according to the AGB models, suggests that the determination of N abundances in the *H*-band for GC giants should be revisited. Such data may be provided by the ongoing APOGEE-2 survey, which is almost triplicating the number of GC stars observed in the *H*-band and continuously improving the precision/reliability of the derived abundances.

ACKNOWLEDGEMENTS

FDA, DAGH, TM, and OZ acknowledge support provided by the Spanish Ministry of Economy and Competitiveness (MINECO) under grant AYA-2014-58082-P. DAGH was also funded by the Ramón y Cajal fellowship number RYC-2013-14182. SzM has been supported by the Premium Postdoctoral Research Program of the Hungarian Academy of Sciences, and by the Hungarian NKFI grant K-119517 of the Hungarian National Research, Development and Innovation Office. Funding for SDSS-III has been provided by the Alfred P. Sloan Foundation, the Participating Institutions, the National Science Foundation, and the U.S. Department of Energy Office of Science. The SDSS-III website is http://www.sdss3.org/. SDSS-III is managed by the Astrophysical Research Consortium for the Participating Institutions of the SDSS-III Collaboration including the University of Arizona, the Brazilian Participation Group, Brookhaven National Laboratory, University of Cambridge, Carnegie Mellon University, University of Florida, the French Participation Group, the German Participation Group, Harvard University, the Instituto de Astrofsica de Canarias, the Michigan State Notre Dame JINA Participation Group, Johns Hopkins University, Lawrence Berkeley National Laboratory, Max Planck Institute for Astrophysics, New Mexico State University, New York University, Ohio State University, Pennsylvania State University, University of Portsmouth, Princeton University, the Spanish Participation Group, University of Tokyo, University of Utah, Vanderbilt University, University of Virginia, University of Washington, and Yale University.

REFERENCES

Alves-Brito A., Schiavon R. P., Castilho B., Barbuy B., 2008, A&A, 486, 941
Arnould M., Goriely S., Jorissen A., 1999, A&A, 347, 572
Bedin L. R., Piotto G., Anderson J., Cassisi S., King I. R., Momany Y., Carraro G., 2004, ApJ, 605, L125
Blöcker T., Schöenberner D., 1991, A&A, 244, L43
Boberg O. M., Friel E. D., Vesperini E., 2016, ApJ, 824, 5
Boesgaard A. M., King J. R., Cody A. M., Stephens A., Deliyannis C. P., 2005, ApJ, 629, 832
Bragaglia A. et al., 2010, LApJ, 720, 41
Caloi V., D'Antona F., 2005, A&A, 435, 987
Caloi V., D'Antona F., 2007, A&A, 463, 949
Caloi V., D'Antona F., 2008, ApJ, 673, 847
Caloi V., D'Antona F., 2011, MNRAS, 417, 228
Canuto V. M. C., Mazzitelli I., 1991, ApJ, 370, 295
Carretta E., 2006, AJ, 131, 1766
Carretta E. et al., 2009a, A&A, 505, 117
Carretta E., Bragaglia A., Gratton R., Lucatello S., 2009b, A&A, 505, 139
Charbonnel C., Lagarde N., 2010, A&A, 522, A10

Cohen J. G., Briley M. M., Stetson P. B., 2005a, AJ, 130, 1177
Cohen J. G., Meléndez J., 2005b, AJ, 129, 303
Cristallo S., Straniero O., Piersanti L., Gobrecht D., 2015, ApJS, 219, 40
D'Antona F., Caloi V., 2004, ApJ, 611, 871
D'Antona F., Caloi V., 2008, MNRAS, 390, 693
D'Antona F., Ventura P., 2007, MNRAS, 379, 1431
D'Antona F., Caloi V., Montalbán J., Ventura P., Gratton R., 2002, A&A, 395, 69
D'Ercole A., Vesperini E., D'Antona F., McMillan S. L. W., Recchi S., 2008, MNRAS, 391, 825
D'Ercole A., D'Antona F., Vesperini E., 2011, MNRAS, 415, 1304
D'Ercole A., D'Antona F., Vesperini E., 2016, MNRAS, 461, 4088
Dalessandro E., Salaris M., Ferraro F. R., Mucciarelli A., Cassisi S., 2013, MNRAS, 430, 459
De Mink S. E., Pols O. R., Langer N., Izzard R. G., 2009, A&A, 507, L1
Denissenkov P. A., Hartwick F. D. A., 2014, MNRAS, 437, L21
Denissenkov P., VandenBerg D. A., Kopacki G., Ferguson J. W., 2017, ApJ, 849, 159
Di Criscienzo M. et al., 2011, MNRAS, 414, 3381
Dobrovolskas V., Kucinskas A., Bonifacio P., Caau E., Ludwig H. G., Steen M., Spite M., 2015, A&A, 576, A128
D'Ercole A., D'Antona F., Ventura P., Vesperini E., McMillan S. L. W., 2010, MNRAS, 407, 854
Fishlock C. K., Karakas A. I., Lugaro M., Yong D., 2014, ApJ, 797, 44
Gratton R. G. et al., 2001, A&A, 369, 87
Gratton R. G., Sneden C., Carretta E., 2004, ARA&A, 42, 385
Gratton R. G., Carretta E., Bragaglia A., 2012, ARA&A, 20, 50
Gratton R. G. et al., 2013, A&A, 549, A41
Hale S. E., Champagne A. E., Iliadis C., Hansper V. Y., Powell D. C., Blackmon J. C., 2002, Phys. Rev. C, 65, 5801
Hale S. E., Champagne A. E., Iliadis C., Hansper V. Y., Powell D. C., Blackmon J. C., 2004, Phys. Rev. C, 70, 5802
Herwig F., 2005, ARA&A, 43, 435
Johnson C. I., Kraft R. P., Pilachowski C. A., Sneden C., Ivans I. I., Benman G., 2005, PASP, 117, 1308
Karakas A. I., Lattanzio J. C., 2014, PASA, 31, e030
Kraft R. P., Sneden C., Smith G. H., Shetrone M. D., Langer G. E., Pilachowski C. A., 1997, AJ, 113, 279
Krause M., Charbonnel C., Decressin T., Meynet G., Prantzos N., 2013, A&A, 552, A121
Lardo C. et al., 2013, MNRAS, 433, 1941
Lee J.-W., 2017, ApJ, 844, 77
Lodders K., 2003, ApJ, 591, 1220
Majewski S. R. et al., 2017, AJ, 154, 46
Massari D., Lapenna E., Bragaglia A., Dalessandro E., Contreras Ramos R., Amigo P., 2016, MNRAS, 458, 4162
Mészáros S. et al., 2015, AJ, 149, 153 (ME15)
Milone A. P. et al., 2014, ApJ, 785, 21
Milone A. P. et al., 2015, MNRAS, 447, 927
Milone A. P. et al., 2017, MNRAS, 464, 3636
Pancino E. et al., 2017, A&A, 601, 112
Piotto G. et al., 2007, ApJ, 661, L53
Renzini A., Voli M., 1981, A&A, 94, 175
Renzini A. et al., 2015, MNRAS, 454, 4197
Sneden C., Kraft R. P., Guhathakurta P., Peterson R. C., Fulbright J. P., 2004, AJ, 127, 2162
Valcarce A. A. R., Catelan M., Alonso-García J., Contreras Ramos R., Alves S., 2016, A&A, 589, A126
VandenBerg D. A., Denissenkov P. A., Catelan M., 2016, ApJ, 827, 2
Ventura P., 2010, Light Elements in the Universe. Proc. IAU Symp. 268. Cambridge Univ. Press, Cambridge, p. 147
Ventura P., D'Antona F., 2005, A&A, 431, 279
Ventura P., D'Antona F., 2006, A&A, 457, 995
Ventura P., D'Antona F., 2009, MNRAS, 499, 835
Ventura P., Zeppieri A., Mazzitelli I., D'Antona F., 1998, A&A, 334, 953
Ventura P., Carini R., D'Antona F., 2011, MNRAS, 415, 3865
Ventura P., Di Criscienzo M., Carini R., D'Antona F., 2013, MNRAS, 431, 3642
Ventura P. et al., 2016, ApJ, 831, L17
Vesperini E., McMillan S. L. W., D'Antona F., D'Ercole A., 2013, MNRAS, 429, 1913
Villanova S., Geisler D., 2011, A&A, 535, A31
Villanova S., Geisler D., Carraro G., Moni Bidin C., Muñoz C., 2013, ApJ, 778, 186
Yong D. et al., 2014, MNRAS, 441, 3396

This paper has been typeset from a TEX/LATEX file prepared by the author.